JOURNAL OF GEOPHYSICAL RESEARCH, VOL. 115, B03104, doi:10.1029/2009JB006475, 2010

Assessment of the usefulness of lithic clasts from pyroclastic deposits for paleointensity determination

Greig A. Paterson,[1] Adrian R. Muxworthy,[2] Andrew P. Roberts,[1] and Conall Mac Niocaill[3]

Received 20 March 2009; revised 20 August 2009; accepted 1 October 2009; published 26 March 2010.

[1] Paleomagnetic and rock magnetic measurements were carried out on lithic clasts found within pyroclastic deposits to assess their potential for paleointensity determinations. The use of multiple lithologies in a single paleointensity determination would provide confidence that the result is not biased by alteration within one lithology. Lithic clasts were sampled from three historically active volcanoes: Láscar in the Chilean Andes, Mt. St. Helens, United States, and Vesuvius, Italy. At Láscar, triple heating paleointensity experiments allow development of new selection criteria for lithic clasts found within pyroclastic deposits. Using these criteria, the Láscar data yield a mean paleointensity of 24.3 ± 1.3 μT (1σ, N = 26), which agrees well with the expected value of 24.0 μT. This indicates that pyroclastic rocks have promise for paleointensity determinations. Pyroclastics, however, still suffer from the range of problems associated with conventional paleointensity experiments on lava flows. Samples from Mt. St. Helens are strongly affected by multidomain (MD) behavior, which results in all samples failing to pass the paleointensity selection criteria. At Vesuvius, MD grains, magnetic interactions, and chemical remanent magnetizations contributed to failure of all paleointensity experiments. Rock magnetic analyses allow identification of the causes of failure of the paleointensity experiments. However, in this study, they have not provided adequate preselection criteria for identifying pyroclastics that are suitable for paleointensity determination.

Citation: Paterson, G. A., A. R. Muxworthy, A. P. Roberts, and C. Mac Niocaill (2010), Assessment of the usefulness of lithic clasts from pyroclastic deposits for paleointensity determination, *J. Geophys. Res.*, *115*, B03104, doi:10.1029/2009JB006475.

1. Introduction

[2] Information about the full paleomagnetic vector can give insights into the workings of the geomagnetic field as well as an understanding of the evolution of the Earth's core. Determining the strength of the paleomagnetic field, however, is problematical. Absolute paleointensity experiments are time consuming and prone to failure, which makes it difficult to obtain good data. This limits the global paleointensity database, which has inadequate spatial and temporal resolution [*Perrin and Schnepp*, 2004]. Failure to experimentally determine the paleointensity of a sample can result from numerous factors, with alteration in nature or during laboratory heating, and the influence of multidomain (MD) grains being the most commonly cited problems [e.g., *Levi*, 1977; *Perrin*, 1998; *Carvallo et al.*, 2006; *Tarduno et al.*, 2006]. Developing reliable yet efficient experimental techniques is important for improving paleointensity data quality [e.g., *Thellier and Thellier*, 1959; *Coe*, 1967a; *Shaw*, 1974; *Walton et al.*, 1992; *Yu et al.*, 2004; *Dekkers and Böhnel*, 2006], as is expanding the range of materials to investigate [e.g., *Pick and Tauxe*, 1993; *Cottrell and Tarduno*, 1999; *Ben-Yosef et al.*, 2008]. Characterizing and understanding the behavior of previously rarely used materials enables assessment of their potential usefulness as paleomagnetic recorders. Pre-existing lithic fragments that are reheated as they are incorporated into pyroclastic density currents (PDCs), and their subsequent deposits are one such material. Reheating during eruption partially resets the magnetization of these clasts to record the ambient field at the time of eruption. The explosive nature of volcanic eruptions associated with PDCs frequently results in a range of lithic fragments being incorporated into deposits and the high temperatures involved (up to about 1200°C) [*Fisher and Schmincke*, 1984] can often fully reset the magnetization. The nature of deposition of these clasts allows consistency checks to be made. Clasts emplaced at varying temperatures give confidence that the magnetic remanence is of thermal rather than chemical origin. The multiple lithologies in these deposits provides a further check against chemical alteration, where consistent results from different lithologies give greater confidence in the result.

[3] Pyroclastic deposits have been studied using paleomagnetism to investigate secular variation [e.g., *Lanza and Zanella*, 2003] or the emplacement temperature of the deposits [e.g., *Kent et al.*, 1981], but relatively few paleo-

[1]National Oceanography Centre, University of Southampton, Southampton, UK.
[2]Department of Earth Science and Engineering, Imperial College London, London, UK.
[3]Department of Earth Sciences, University of Oxford, Oxford, UK.

0148-0227/10/2009JB006475

Table 1. Definitions of the Investigated Experimental Paleointensity Selection Criteria

Criterion	Definition
q	Quality factor: a measure of the overall quality of the paleointensity estimate [*Coe et al.*, 1978]
f	NRM fraction used for the best-fit on an Arai diagram
N	Number of data points used for the paleointensity estimate
β	Ratio of the standard error of the slope to the absolute value of the slope
MAD	Maximum angular deviation of the anchored fit to the paleomagnetic vector on a vector component diagram
α	Angular difference between the anchored and free-floating vectors on a vector component diagram
DRAT	Maximum difference produced by a pTRM check, normalized by the length of the line segment
$\text{DRAT}_{\text{Tail}}$	Maximum difference produced by a pTRM tail check, normalized by the length of the line segment
δ(CK)	Maximum difference produced by a pTRM check, normalized by the TRM (obtained from the intersection of the best-fit line and the x-axis on an Arai plot)
δ(TR)	Maximum difference produced by a pTRM tail check, normalized by the initial NRM
$\delta(t^*)$	Extent of pTRM tail after correction for angular dependence

intensity studies have been carried out, and none have assessed their viability for paleointensity determinations using historic samples. The youngest pyroclastic lithic clasts from which paleointensity estimates have been made are dated at about 3600 years B.P., where paleointensity experiments were used to assess the reliability of emplacement temperature determinations for pyroclastic deposits from Santorini, Greece [*Bardot and McClelland*, 2000]. Of the 24 samples measured, seven gave acceptable paleointensity results. One sample from ~3600 years B.P. eruption gave an estimate that was comparable with paleointensity values from archaeomagnetic studies. The remaining six samples were from older deposits (21,000–180,000 years B.P.) and their results were compared with virtual dipole moment curves from sedimentary records [*Guyodo and Valet*, 1996]. Uncertainties associated with age estimations for these eruptions makes the comparisons inconclusive. The small data set, and both age and paleofield uncertainties make the study of *Bardot and McClelland* [2000] an inadequate assessment of the potential usefulness of pyroclastic lithics as paleointensity recorders. In this paper, we consider lithic clasts from three historical pyroclastic eruptions in order to test their potential use for paleointensity analysis, and to test the effectiveness of previously published paleointensity selection criteria. Various rock magnetic parameters have also been investigated to assess their usefulness as preselection criteria for absolute paleointensity studies.

2. Sampling and Experimental Procedures

[4] The three volcanoes from which historical pyroclastic deposits were studied are: Volcán Láscar, Chile, Mt. St. Helens, United States, and Vesuvius, Italy. At all localities sampled in this study, oriented-hand samples were collected using the method described by *Tarling* [1983]. A magnetic compass-clinometer was used for sample orientation. Cores with 10 or 20 mm diameter were then drilled from the sampled clasts in the laboratory. Remanence measurements were made within a magnetically shielded laboratory using either a 2-G Enterprises cryogenic magnetometer, an Agico JR5A spinner magnetometer, or a Molspin Minispin magnetometer at the National Oceanography Centre, Southampton (NOCS). Thermal treatment was carried out using an ASC Scientific oven, which has a residual field of less than 50 nT, and an applied field control of $<\pm 0.5$ μT. Either the Coe paleointensity method, with partial thermoremanent magnetization (pTRM) checks and pTRM tail checks, with an applied field of 30 μT [*Coe*, 1967a; *McClelland and Briden*, 1996], or the IZZI protocol [*Yu et al.*, 2004; *Yu and Tauxe*, 2005], including pTRM tail checks, with an applied field of 10 μT, were used. Low-field magnetic susceptibility was measured at room temperature after each heating step using a Bartington Instruments MS2B magnetic susceptibility meter. Data analysis was performed using the ThellierTool v4.2 software [*Leonhardt et al.*, 2004a]. The error associated with paleointensity estimates from historic eruptions can be quantified by the intensity error fraction, IEF(%):

$$\text{IEF}(\%) = \frac{I_{\text{Meas}} - I_{\text{Exp}}}{I_{\text{Exp}}} \times 100, \quad (1)$$

where I_{Meas} and I_{Exp} are the measured and expected geomagnetic field strengths, respectively. Various experimental parameters are typically used to quantify the quality of, and to select, paleointensity data [e.g., *Coe et al.*, 1978]. Definitions of the main parameters used in this study are briefly summarized in Table 1.

[5] Sister samples from every studied clast were cut for rock magnetic measurements. Hysteresis loops, back-field demagnetization curves, first-order reversal curve (FORC) diagrams and thermomagnetic curves were measured using a Princeton Measurements Corporation Vibrating Sample Magnetometer (VSM) at NOCS (maximum applied field of 1 T). An Agico KLY-2 Kappabridge magnetic susceptibility meter with furnace attachment was used to measure susceptibility-temperature curves at the University of Oxford. Stepwise alternating field (AF) demagnetization was carried out on additional sister samples up to a maximum peak field of 140 mT, and the remanence was measured using the 2-G Enterprises magnetometer at NOCS. FORC diagrams were produced using the FORCinel v1.11 software [*Harrison and Feinberg*, 2008]. Thermomagnetic curves were analyzed using the second derivative approach as implemented by the RockMag Analyzer software v1.0 [*Leonhardt*, 2006], and susceptibility-temperature curves were analyzed using the inverse susceptibility method outlined by *Petrovský and Kapička* [2006].

3. Volcán Láscar, Chile

3.1. Background

[6] Láscar is a stratovolcano in the Chilean Andes, near the Argentinean border. On April 18, 1993, Láscar erupted for 3 days, in what was the largest historic eruption in the northern Andes [*Smithsonian Institution*, 1993]. Two intense eruptions on April 19, 1993 produced ejecta columns as high

Table 2. Paleointensity Data Obtained From Láscar, Chile[a]

Sample	Clast Type	Selected	Intensity (μT)	IEF (%)	ΔT (°C)	N	β	f	q	δ(CK)	δ(TR)	MAD Anc.	α
LV3B3	Reddened andesite	N	17.5	−27.21	100–620	16	0.02	0.97	37.6	4.4	7.0	7.6	3.5
LV4A3	Reddened andesite	Y	24.6	2.58	100–600	15	0.03	0.62	18.7	1.6	4.4	1.3	2.6
LV4C3	Andesite	Y	23.9	−0.42	260–460	5	0.01	0.76	64.9	2.2	1.5	0.8	0.8
LV6A2	Andesite	N	47.6	98.25	420–620	9	0.02	0.97	45.3	12.1	9.7	1.6	0.9
LV6C3A	Andesite	Y	23.7	−1.08	100–580	13	0.02	0.97	31.4	5.0	5.9	2.0	1.0
LV6D1B	Andesite	Y	25.4	5.71	260–460	5	0.02	0.81	23.0	6.4	1.6	1.7	1.4
LV6G1	Andesitic pumice	N	43.4	80.88	100–580	12	0.07	0.93	11.6	27.4	5.4	3.6	4.8
LV6I3A	Andesite	Y	24.8	3.42	220–420	5	0.02	0.81	24.1	7.0	5.1	0.6	0.6
LV7B1	Andesite	N	14.5	−39.75	100–500	10	0.10	0.79	3.8	5.9	6.6	5.0	4.0
LV7G1	Andesite	Y	25.8	7.58	100–420	8	0.10	0.29	2.4	1.3	4.2	2.8	8.9
LV7H1	Andesite	Y	22.5	−6.25	100–460	10	0.02	0.72	20.6	1.7	4.2	1.4	2.2
LV9A2	Dacitic pumice	N	33.0	37.42	140–560	13	0.04	0.92	19.5	11.8	6.7	1.8	0.6
LV9F2	Andesite	Y	25.8	7.29	100–540	13	0.03	1.00	23.0	9.5	2.4	1.7	0.5
LV10D3A	Dacitic pumice	N	24.5	2.00	140–500	10	0.11	0.26	1.4	4.0	1.3	1.2	1.9
LV11A2	Andesite	Y	24.9	3.92	100–580	14	0.01	0.98	55.4	8.0	4.8	1.4	0.6
LV12A2A	Reddened andesite	Y	23.2	−3.33	100–420	9	0.02	0.48	18.1	3.3	1.6	1.8	5.4
LV12D1	Dacite	Y	24.1	0.37	300–500	6	0.03	0.83	17.2	6.6	3.3	1.2	0.9
LV12E2	Reddened andesite	Y	24.1	0.29	100–560	14	0.02	0.87	41.6	1.9	5.9	3.0	6.1
LV14C3A	Dacitic pumice	N	15.1	−37.00	100–460	10	0.03	0.75	15.0	14.4	8.1	2.3	0.9
LV15B1	Dacite	Y	23.1	−3.79	260–460	6	0.04	0.67	12.6	5.2	4.7	1.6	0.6
LV16A2B	Dacite	N	15.5	−35.29	100–580	13	0.05	0.94	13.8	22.0	3.2	3.0	2.9
LV16B1B	Andesite	N	24.2	0.92	100–540	12	0.11	0.87	5.6	7.1	13.2	2.3	0.2
LV17A1A	Andesite	Y	26.2	9.04	220–500	8	0.01	0.95	55.3	6.7	1.3	0.8	0.3
LV18B3	Andesite	Y	22.2	−7.46	100–580	13	0.06	1.00	13.4	10.0	6.4	3.6	1.2
LV19A2	Dacite	Y	24.0	−0.04	100–540	12	0.02	0.93	38.5	7.8	6.4	1.3	0.5
LV19B1A	Dacite	Y	24.3	1.04	100–460	10	0.04	0.31	5.2	2.2	2.9	0.9	1.4
LV19C1	Andesite	N	24.7	2.88	100–460	10	0.04	0.70	10.4	3.3	8.5	1.3	0.3
LV19D3	Andesite	N	20.5	−14.54	100–580	13	0.03	0.97	24.5	16.0	6.6	1.4	0.2
LV19E1	Dacite	N	12.8	−46.50	100–460	10	0.04	0.65	10.9	3.2	6.7	2.7	5.8
LV19F2	Dacite	Y	25.1	4.46	100–460	10	0.01	0.85	56.0	7.1	1.8	0.9	0.5
LV19G2B	Dacite	Y	25.2	5.17	100–540	12	0.06	0.97	13.7	8.1	5.4	1.7	1.9
LV20B1	Dacite	Y	23.0	−4.38	100–540	12	0.02	0.96	37.3	4.6	2.8	1.0	0.6
LV20C2	Dacite	Y	24.3	1.21	300–580	8	0.03	0.98	26.2	5.4	3.1	1.4	0.5
LV21A2	Andesite	Y	23.3	−2.75	100–560	13	0.03	0.93	27.8	4.4	1.9	1.6	1.3
LV21B1	Dacite	N	25.9	8.08	100–580	13	0.03	0.96	24.2	2.6	8.5	1.6	1.1
LV21C1	Andesite	Y	22.6	−5.83	100–580	15	0.03	0.97	24.1	7.3	2.5	2.0	1.8
LV22D1	Andesite	N	20.7	−13.67	100–500	11	0.06	0.93	11.5	5.2	7.4	5.6	8.5
LV23A2	Andesite	N	24.0	0.13	100–580	13	0.17	0.62	1.7	22.7	5.8	4.9	2.2
LV25C3	Dacite	Y	26.9	12.00	220–580	12	0.02	0.96	43.4	5.3	2.8	2.0	0.6
LV26D2	Andesite	N	12.6	−47.58	100–500	11	0.20	0.72	2.6	13.7	16.9	4.8	3.0
LV27B2	Dacite	N	21.1	−12.08	100–540	12	0.05	0.89	13.0	14.6	8.3	1.4	1.2
LV28E3A	Andesite	N	25.0	4.25	100–460	10	0.06	0.91	12.3	2.5	15.6	1.3	0.7
LV29B2A	Andesite	N	18.4	−23.33	100–580	13	0.03	0.87	21.7	11.2	10.3	3.2	2.7
LV30A3A	Andesitic pumice	Y	23.6	−1.58	100–420	9	0.06	0.78	4.3	8.6	4.5	3.6	5.1
LV30B2	Dacite	N	27.8	16.00	100–580	13	0.03	0.96	26.3	9.8	12.6	1.8	0.5
LV30D1	Andesite	Y	26.2	9.00	100–420	9	0.04	0.85	13.2	3.0	4.6	1.2	1.0

[a]ΔT is the temperature interval for the best-fit line on the Arai plot. MAD Anc. is the MAD for an anchored best fit.

as 22 km. PDCs resulted on 19 and 20 April 1993, respectively, following the collapse of eruptive columns. A total of 111 clasts, representing 31 sites from pyroclastic deposits on the northern and southern flanks of Láscar, were investigated to determine the emplacement temperature of the deposits [*Paterson et al.*, 2010]. The sampled lithic clasts are andesitic to dacitic in composition. Paleomagnetically determined emplacement temperatures indicate that the clasts were heated above the Curie temperature (T_c) of the constituent magnetic minerals (397°C–641°C). Only clasts that record paleomagnetic directions within 30° of the expected geomagnetic field direction were used to estimate the emplacement temperature; 72 independent clasts passed this criterion. Twenty-seven of the clasts have self-reversing magnetizations [*Paterson et al.*, 2010], which makes them unsuitable for paleointensity determination. Forty-six clasts were subjected to paleointensity analysis, including an additional clast (LV19A), which was unavailable for emplacement temperature determination. Three main clast types were analyzed: andesites, reddened andesites, and dacites. The strength of the geomagnetic field at Láscar during April 1993 was 24.0 μT [*IAGA*, 2005].

3.2. Results

[7] The Coe protocol [*Coe*, 1967a] with pTRM check and pTRM tail checks, and an applied field of 30 μT was used to obtain paleointensity estimates from the Láscar samples. In order to obtain a best-fit line on Arai plots, initial selection criteria were applied ($f \geq 0.1$, $\beta \leq 0.3$, $N \geq 4$; see Table 1 for definitions of these parameters). These criteria are less strict than those typically applied when estimating a final paleointensity value [e.g., *Selkin and Tauxe*, 2000; *Kissel and Laj*, 2004]. The lowest permitted temperature step was 100°C, to exclude potential viscous overprints. All 46 samples pass the initial criteria; Table 2 contains the full results of the paleointensity analysis, and example Arai plots are shown in Figures 1a–1d. The data yield a mean intensity value that is consistent with the expected field intensity

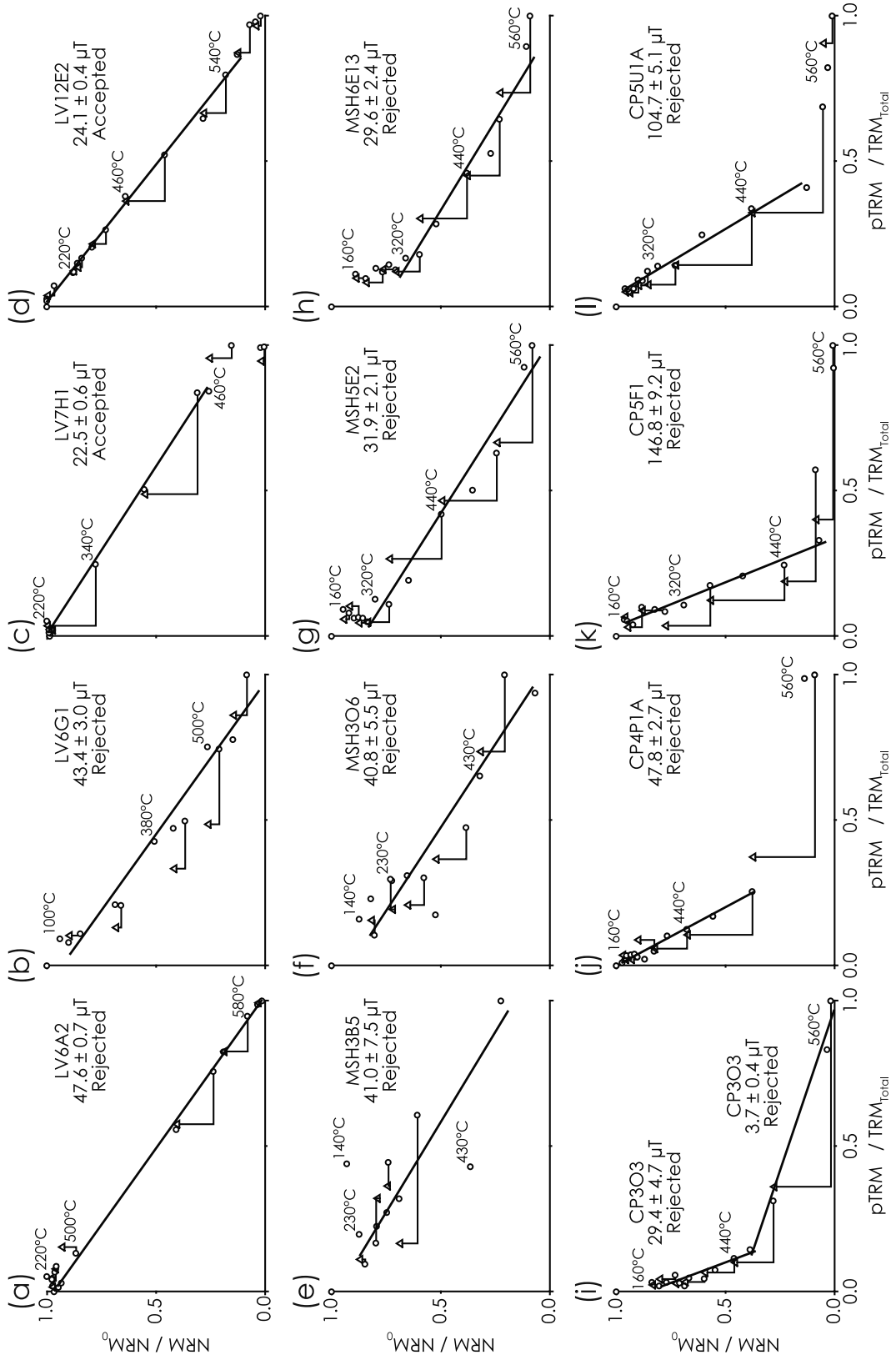

Figure 1. Typical Arai plots for clasts from pyroclastic deposits from (a–d) Láscar, (e–h) Mt. St. Helens, and (i–l) Vesuvius. Circles represent NRM-TRM data points; triangles represent pTRM checks. Samples labeled as "Accepted" or "Rejected" refer to whether the sample passed the final selection criteria outlined in section 6 and Table 3.

(Int. = 24.0 μT, IEF = 0.0%, σ = 6.10, N = 46, $N(|\text{IEF}| \leq 10\%)$ = 31). The scatter of the intensity values, however, is high ($\delta B\% = \sigma_B/\overline{B} = 25.4\%$), and fails to pass a typically applied threshold of $\delta B\% \leq 25\%$ [*Selkin and Tauxe*, 2000]. Application of stricter paleointensity criteria is discussed in section 6.

4. Mt. St. Helens, United States

4.1. Background

[8] Mt. St. Helens is located in the Cascade Mountain Range of the western United States, and is famous for its devastating eruption on 18 May 1980. This eruptive phase began in late March of 1980 with a series of generally short-lived eruptions. A magnitude 5.1 earthquake on May 18 triggered a landslide that caused rapid depressurization of the northern flank of the volcano, which triggered a lateral surge cloud. Activity continued at Mt. St. Helens during 1980 and the collapse of eruptive columns generated numerous PDCs and deposits [*Smithsonian Institution*, 1980]. One-hundred-thirteen clasts were collected from six sites on the northern flank of Mt. St. Helens. The lithic clasts include basalts, andesites, and dacites. Only four of the six sampled sites were emplaced at high temperatures, with clasts being emplaced at temperatures from 520°C to above the T_c, which ranges from 447°C to 634°C [*Paterson et al.*, 2010]. Sixty-two clasts were determined to have been emplaced at high temperature. The strength of the 1980 geomagnetic field at Mt. St. Helens was 55.6 μT [*IAGA*, 2005].

4.2. Results

[9] The IZZI protocol was applied to one sample from each of the 62 clasts; 6 replicate samples were measured using the triple heating method. Forty samples (39 independent clasts) pass the initial selection criteria, as described in section 3.2 (Figures 1e–1h). These data yield a poorly constrained and inaccurate mean paleointensity (Int. = 44.4 μT, IEF = −20.1%, σ = 14.4, $\delta B\%$ = 32.4%, N = 40, $N(|\text{IEF}| \leq 10\%)$ = 6). The 22 samples that fail to pass initial selection typically fail because of a high β value, as a result of a high degree of scatter, or zigzagging, on the Arai plot. Only one sample subjected to the IZZI protocol passes the typically used criterion of $\beta \leq 0.1$; the six triple heated samples pass this criterion. The failure of β for the IZZI samples suggests that alteration and MD grains have affected the samples.

5. Vesuvius, Italy

5.1. Background

[10] One-hundred twenty-four lithic clasts were sampled at six sites from the 472 A.D. deposits found within the Pollena quarry, on the western flank of Vesuvius [*Paterson et al.*, 2010]. The sampled clasts are predominantly leucite-bearing tephrites, with occasional andesites and a syenite [*Paterson et al.*, 2010]. Sixty-three clasts recorded a direction that is consistent with previously published data (within 30° of the mean paleomagnetic direction). *Paterson et al.* [2010] presented thermomagnetic evidence of the inversion of maghemite, which suggests that the remanent magnetization of two clasts was of chemical, rather than thermal origin (e.g., sample CP6P; Figure 2h); these samples were excluded from emplacement temperature determination and are excluded from the paleointensity analysis. Sixty-one clasts were determined to have been emplaced above ambient temperature. Of these, 41 clasts had been fully remagnetized ($\geq T_c$ = 533°C–649°C) and 20 had been partially remagnetized up to temperatures of 280°C–520°C. On the basis of the CALS7K.2 archaeomagnetic model [*Korte and Constable*, 2005], the field intensity at Vesuvius in 472 A.D. was about 58 μT. A search of the GEOMAGIA database v.2 [*Korhonen et al.*, 2008] for paleo- and archaeointensity estimates using Thellier-type or microwave protocols that include pTRM checks with three or more samples, yields seven estimates from Europe for the time period 413–550 A.D. These paleofield strength estimates correspond to virtual axial dipole moments (VADMs) that range from 9.22 to 10.56 × 10^{22} Am^2 [*Kovacheva and Toshkov*, 1994; *Chauvin et al.*, 2000; *Genevey and Gallet*, 2002; *Genevey et al.*, 2003; *Leonhardt et al.*, 2006]. The corresponding VADM from the CALS7K.2 model data for Vesuvius is 9.92 × 10^{22} Am^2. If we consider the range of values obtained from previous studies as the uncertainty range for the CALS7K.2 estimate, the accuracy is about ±4 μT. This overlaps with the lower end of the VADM estimate of *Knudsen et al.* [2008] for this time interval (10.38–11.12 × 10^{22} Am^2, 60.7–65.0 μT).

5.2. Results

[11] Of the 61 samples subjected to triple heating paleointensity experiments, 56 pass the initial selection criteria. Like the data from Mt. St. Helens, these results provide an inaccurate and poorly constrained intensity estimate (Int. = 45.5 μT, IEF = −22.0%, σ = 29.4, $\delta B\%$ = 64.6%, N = 56, $N(|\text{IEF}| \leq 10\%)$ = 7). The five samples that fail the initial criteria either fail to unblock enough of the NRM up to the temperature at which they were remagnetized (failing the $f \geq 0.1$ criterion) or they fail the $\beta \leq 0.3$ criterion. Representative Arai plots from the Vesuvius samples are shown in Figures 1i–1l.

6. Discussion: Paleointensity Results

6.1. Paleointensity Data

[12] With the least stringent selection criteria, the Láscar data yield an accurate average intensity estimate, but with scattered results. The effects of applying a range of published selection criteria to these paleointensity data are investigated in Figure 3. Owing to the nature of the pTRM checks used, cumulative alteration checks could not be meaningfully applied (i.e., cumulative checks are only valid if the combined checks span the full temperature range of interest, which is not the case here, e.g., Figure 1d). The default "B" class criteria of the ThellierTool [*Leonhardt et al.*, 2004a], the criteria of *Biggin et al.* [2007a] (SELCRIT2, based on the criteria of *Selkin and Tauxe* [2000] with an added MD check), and PICRIT [*Kissel and Laj*, 2004] were all investigated. Each set of criteria yields good paleointensity estimates ($|\text{IEF}| \leq 4.2\%$), which pass a within-site scatter criterion of ≤25%. The ThellierTool "B" class criteria give the lowest scatter (15.4%). This reduced scatter is predominantly the result of exclusion of one sample (LV6A2; Figure 1a), which overestimates the geomagnetic field intensity by >98%. Sample LV6A2 has a large pTRM tail at the 500°C temperature step, and the succeeding pTRM check also fails. Given

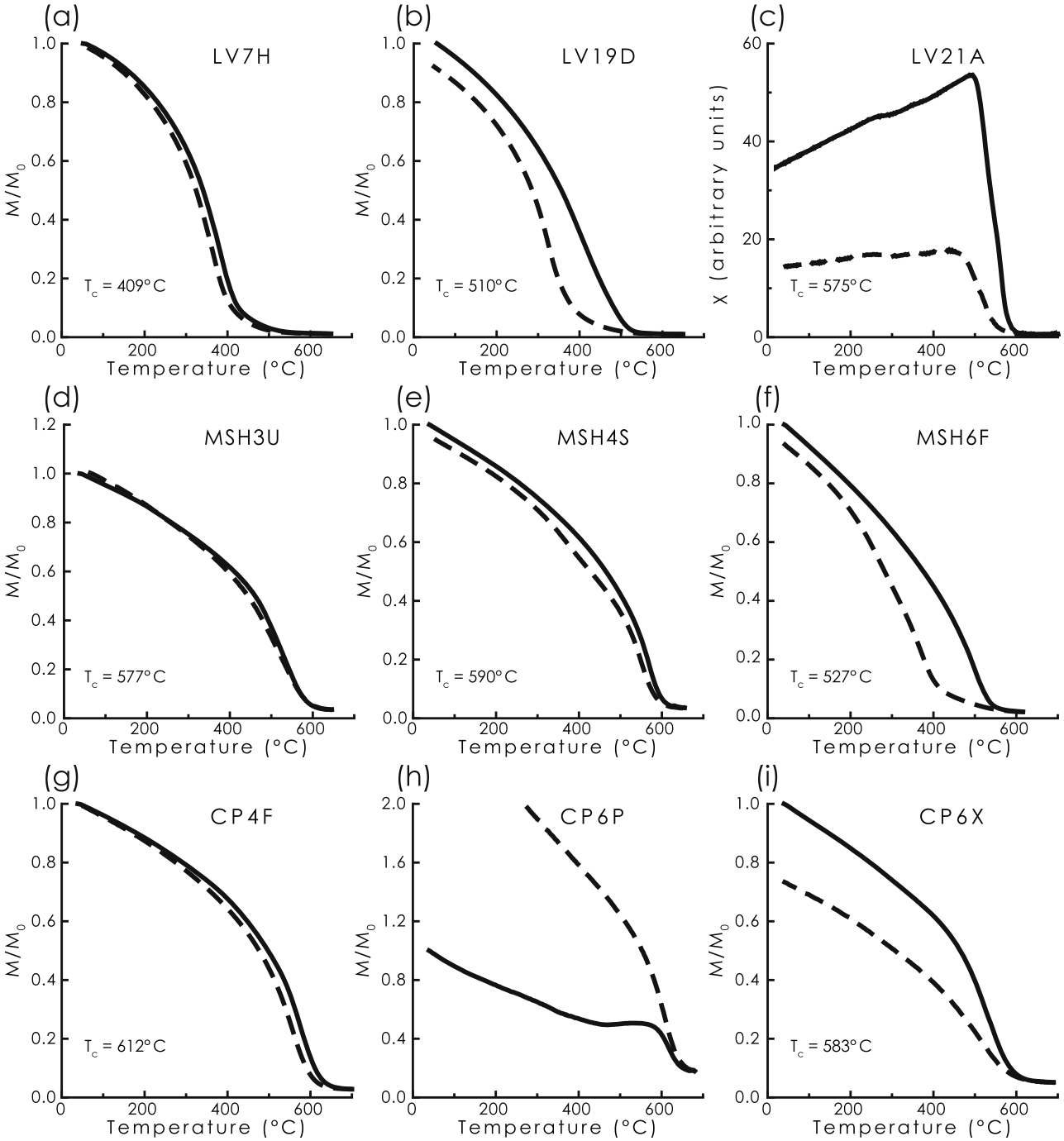

Figure 2. Example thermomagnetic curves from (a–c) Láscar, (d–f) Mt. St. Helens, and (g–i) Vesuvius. Solid (dashed) lines represent the heating (cooling) cycles. The applied field during the experiments was 1 T; heating and cooling rates varied from 10 to 20 °C/min.

that all of the other tail checks are small, it seems likely that this results from chemical alteration during heating. Sample LV6A2 fails the δ(CK) alteration criterion, but passes the difference ratio (DRAT) thresholds of the other selection criteria. The ThellierTool "A" class criteria use a much stricter $\delta(t^*)$ threshold ($\leq$3) and do improve on the result from the "B" criteria by reducing the scatter, but they exclude a further 18 samples (Int. = 23.7 μT, IEF = −1.3%, σ = 0.8, δB% = 3.4%, N = 5, N(|IEF| $\leq$ 10%) = 5).

6.2. Experimental Selection Criteria

[13] As outlined above there are many sets of selection criteria for absolute paleointensity studies, each of which uses slightly different parameters. This raises the question of what threshold values provide the optimal result?

[14] The relationship between various paleointensity selection criteria and IEF(%) was investigated for the Láscar data to determine an optimum set of selection criteria for these pyroclastic materials (Figure 4). The most striking

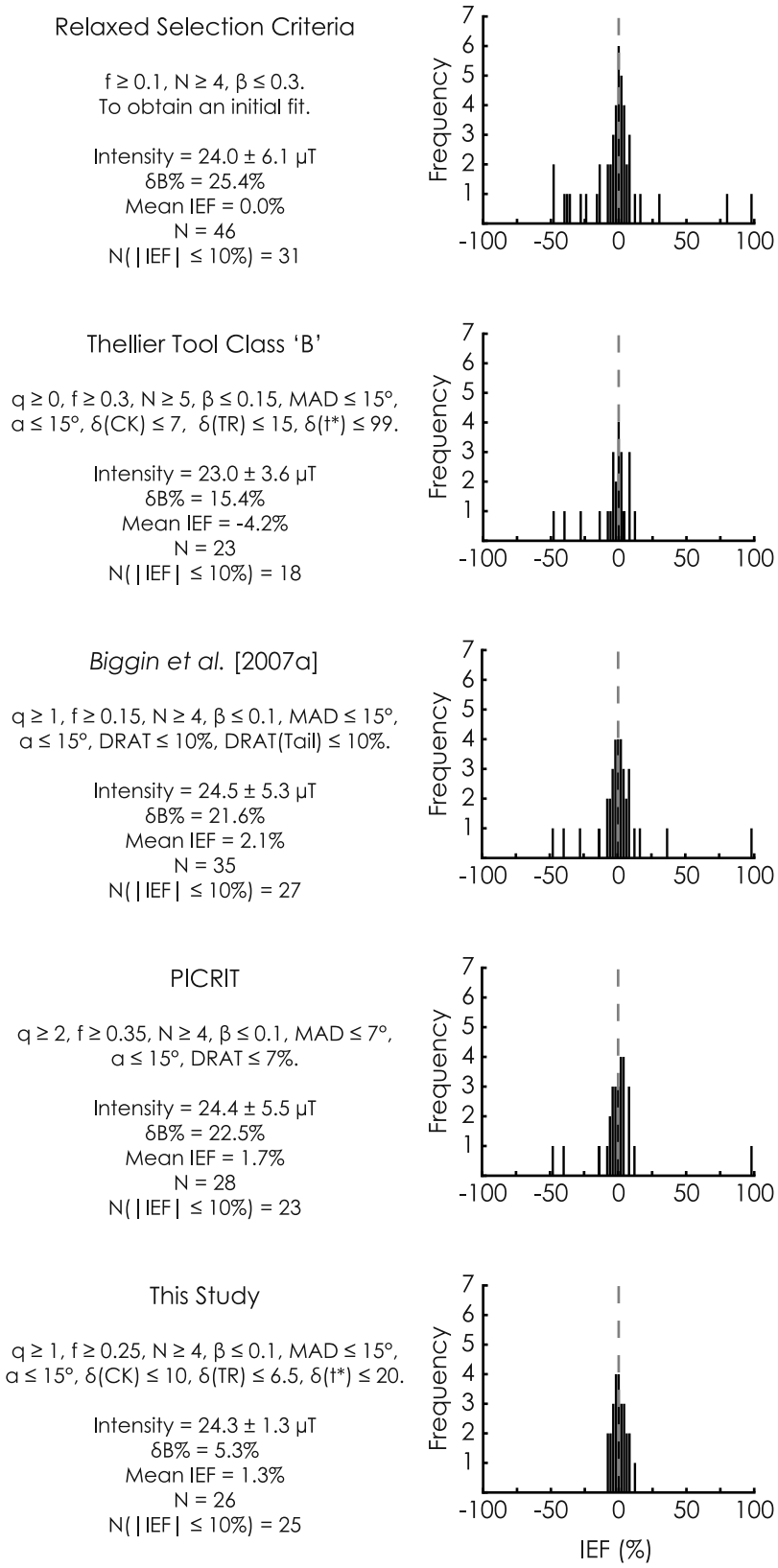

Figure 3. Histograms of paleointensity estimates for the various selection criteria investigated.

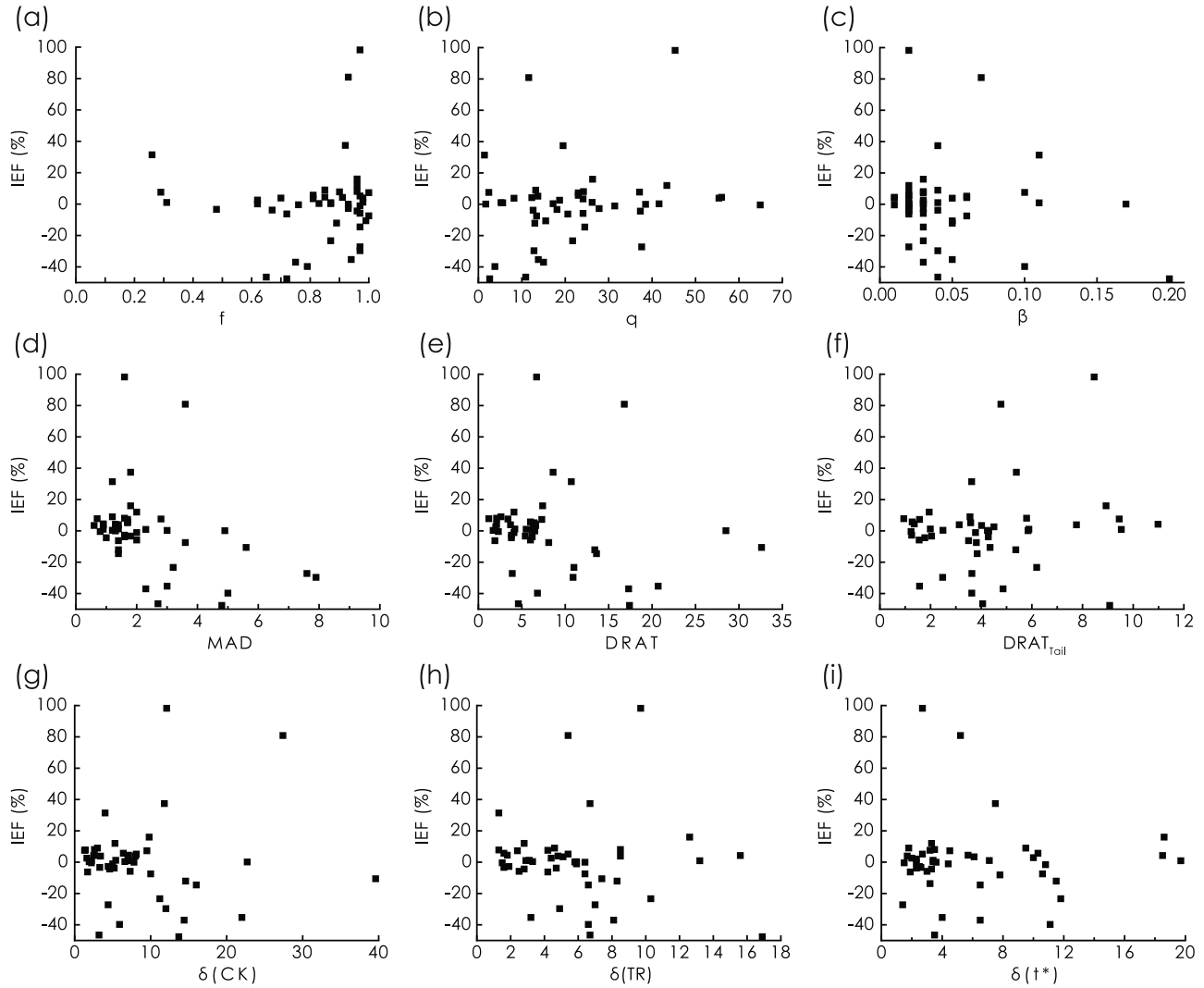

Figure 4. Experimental paleointensity selection criteria for the Láscar samples. These data were used to select cutoff values for acceptable paleointensity results (Figure 3). See Table 1 for a description of these parameters. For clarity, sample LV26D2 (IEF(%) = −47.6, δ(t*) = 102.3) is omitted from Figure 4i.

feature of this analysis is the lack of obvious correlation between the selection criteria and IEF(%). This suggests that the typically used paleointensity selection criteria may not be deterministic. As is the case with most paleointensity studies, threshold values for these criteria were arbitrarily selected. However, knowledge of the correct geomagnetic field intensity value for historic eruptions allows criteria to be chosen to maximize the number of accurate intensity estimates. A key question to address is what normalization best enables identification of alteration and MD magnetizations? *Selkin and Tauxe* [2000] proposed that pTRM checks should be normalized by the length of the line segment used on the Arai plot for their DRAT parameter, while *Biggin et al.* [2007a] normalized pTRM tail checks in the same way for their DRAT$_{Tail}$. *Leonhardt et al.* [2004a] normalized pTRM checks by the TRM (as obtained by the intersection of the best-fit line and the *x*-axis on an Arai plot) and pTRM tail checks by the initial NRM (Table 1).

[15] For the Láscar data, a δ(CK) cutoff of 10% excludes the three most deviant paleointensity estimates, while only excluding two samples with low IEF(%) ($|\text{IEF}| \leq 10\%$; Figure 4g). Similarly, a DRAT cutoff of 10% only excludes two samples with low IEF(%), but it retains the single most deviant result (sample LV6A2; Figure 4e). DRAT < 6.7% is required to exclude the most deviant estimates, but this would also remove five accurate paleointensity estimates. A cutoff value of $\delta(\text{CK}) \leq 10\%$ provides the best reduction of the scatter of estimates while keeping a large number of accurate results. An important factor to consider is the role that *f* plays on DRAT and δ(CK) values. For fractions $\ll 1$, the length of the best-fit line used to normalize the DRAT parameter will be smaller than the TRM value used to calculate δ(CK). The effect is that, for the same absolute value of a pTRM check, the DRAT parameter will be larger than δ(CK), hence δ(CK) should be a more lenient criterion. The majority of Láscar samples have $f > 0.6$, so this effect is unlikely to be significant. In addition, the critical cutoff values for alteration checks are dependent on the experimental setup, particularly the heating step increments. If a sample undergoes gradual alteration and small temperature steps are used, the alteration checks will be smaller than if larger temperature increments are used. In this situation,

Table 3. Paleointensity Selection Criteria for Pyroclastic Lithics[a]

Criterion	Cut-Off Value
q	≥ 1
f	≥ 0.25
N	≥ 4
β	≤ 0.1
MAD	≤ 15
α	≤ 15
δ(CK)	≤ 10
δ(TR)	≤ 6.5
$\delta(t^*)$	≤ 20

[a]This study.

cumulative checks provide the best discrimination against chemical alteration. For Láscar, however, accurate results can be obtained using both DRAT and δ(CK) criteria with different threshold values, which suggests that gradual alteration is unlikely to have occurred with these samples.

[16] In relation to pTRM tail checks, accurate results can be obtained from samples with large $DRAT_{Tail}$ and δ(TR) values (Figures 4f and 4h). Using a 10% cutoff produces better results from δ(TR) simply because it excludes sample LV6A2. To exclude the three most deviant paleointensity results, a $DRAT_{Tail}$ cutoff of $\leq$4.8% or $\delta(TR) \leq 5.4\%$ would be necessary. This is strict for both parameters, but for δ(TR) this cutoff results in exclusion of the seven most deviant results. Relaxing the cutoff to $\delta(TR) \leq 6.5\%$ still excludes around two-thirds of the less accurate results, while retaining over 85% of the accurate estimates. The parameter $\delta(t^*)$ takes into account the angle that the laboratory field makes with the NRM, which is an important consideration for identifying MD pTRM tails. For the Láscar data (Figure 4i), the largest |IEF(%)| is at low (<8) $\delta(t^*)$ values. A few samples have $\delta(t^*)$ about 20 and yet have low IEF(%) values. On the basis of this data set, we have set a critical cutoff of $\delta(t^*) \leq 20$; this is considerably higher than the default value of the ThellierTool class "A" criteria ($\delta(t^*) \leq 3$).

[17] After applying the δ(CK) and δ(TR) criteria, variation of other parameters has little influence on improving the result. We set the parameters to values that are typically used or to the minimum appropriate value observed in the data. The finally adopted selection criteria are listed in Table 3. Applying these criteria significantly reduces the scatter and provides an accurate estimate of the geomagnetic field intensity of 24.3 ± 1.3 μT (Figure 3, Table 4). The scatter (about 5%) is considerably less than that typically observed for paleointensity experiments on historic samples [e.g., *Hill and Shaw*, 2000; *Biggin et al.*, 2007a].

[18] All data from Mt. St. Helens (Figure 5) fail to pass the selection criteria in Figure 3. The fact that most samples fail δ(CK) or DRAT, but pass δ(TR) or $DRAT_{Tail}$, suggests that chemical alteration during heating is responsible for the failure. Although around one-third of the samples are pumiceous, these samples have no bias to higher alteration checks compared to other samples. The failure of the alteration and not the pTRM tail criteria may be an artifact of the low laboratory field strength, which will produce relatively smaller pTRM tails. This can make the δ(TR) and $DRAT_{Tail}$ criteria easier to pass. The low field strength, combined with the IZZI protocol, may also emphasize nonideal MD behavior. The phenomenological model of *Biggin* [2006] suggests that paleointensity experiments using the IZZI protocol with laboratory fields that are much lower than the paleofield can increase the scatter on an Arai plot compared to laboratory fields with similar magnitude to the paleofield. This is in disagreement with the conclusions of *Yu et al.* [2004]. In Figure 6a, the scatter on the Arai plot (β) is plotted against the angle between the laboratory field and the sample NRM. Weak correlation ($R^2 = 0.366$) between the two parameters is still significant at the 0.01 significance level. This suggests that the scatter on the Arai plots is partially due to MD effects. A weak correlation between β and δ(CK) ($R^2 = 0.254$) indicates that thermal alteration during experiments is also a source of scatter on the Arai plots. Reanalysis of $\delta(t^*)$ for all samples (Figure 6b) indicates that the Mt. St. Helens samples have high values, due to the large angle between the applied field and the NRM (Figure 6a). Although, the largest range of IEF(%) values is at low $\delta(t^*)$ values, few samples with $\delta(t^*) > 20$ have low IEF(%) values. This supports the interpretation that the Mt. St. Helens samples failed predominantly due to MD effects. The low laboratory/paleofield ratio (10/55.6) confirms the suggestion that the laboratory field should approximate the paleofield [*Biggin*, 2006].

[19] When the selection criteria tested in Figure 3 are applied to the Vesuvius data (Figure 5), all samples are rejected by the ThellierTool "B" criteria. Four samples remain after applying the criteria of *Biggin et al.* [2007a], but they significantly underestimate the paleointensity, with scattered results (Int. = 23.2 μT, IEF = −60.2%, σ = 15.0, δB% = 64.7%, N = 4, $N(|IEF| \leq 10\%) = 0$). The PICRIT criteria yield an overestimate of the paleointensity with a similar scatter as the unselected data and the *Biggin et al.* [2007a] criteria (Int. = 67.4 μT, IEF = 15.6%, σ = 44.6, $\delta B\%$ = 66.2%, N = 4, $N(|IEF| \leq 10\%) = 0$). Despite yielding "acceptable" results, these data would be rejected after applying a site criterion of $\delta B\% \leq 25\%$. As is the case for the two samples that were initially rejected due to the

Table 4. Paleointensity Results From Láscar, Chile[a]

Group	Mean (μT)	IEF (%) (μ)	n/N	Relative Abundance (%)	σ (μ)	δB (%)
Unselected	24.0	0.0	46/46	–	6.1	25.4
Selected	24.3	1.3	26/46	–	1.3	5.3
Andesites	24.4	1.7	13/23	50.0	1.4	5.7
Reddened andesites	24.0	0.0	3/4	11.5	0.7	2.9
Andesitic pumices	23.6	−1.7	1/2	3.8	–	–
Dacites	24.4	1.7	9/14	34.7	1.2	4.9

[a]N is the total number of samples; n is the number of samples used to calculate the mean paleointensity estimate.

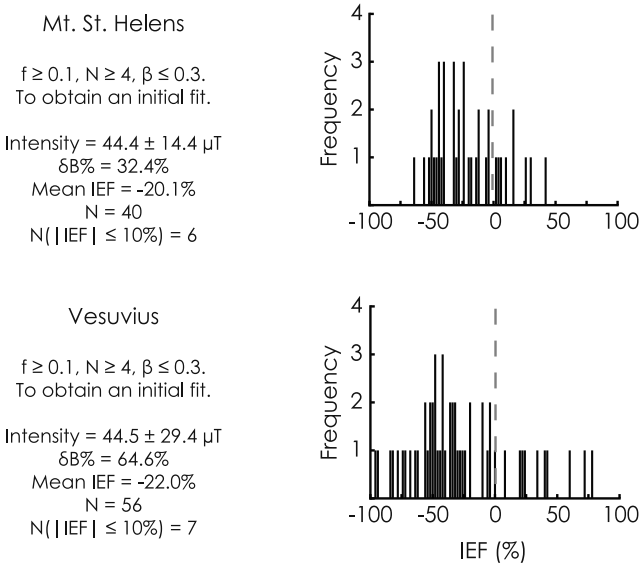

Figure 5. Histograms of paleointensity estimates for Mt. St. Helens and Vesuvius obtained using the relaxed selection criteria. For clarity, Vesuvius sample CP2A2 (IEF = 158%) is omitted.

presence of maghemite, the apparent cause of failure for the Vesuvius samples is predominantly chemical alteration, either in nature or during laboratory heating.

[20] Applying the criteria in Table 3 to the Mt. St. Helens and Vesuvius data results in exclusion of all samples. The majority of the samples fail the δ(CK) $\leq$ 10% or $\delta(t^*) \leq$ 20% criteria for pyroclastic material. Poor data quality prevents an adequate test of our paleointensity selection criteria, or refinement of the cutoff values for the various parameters.

6.3. Chemical Alteration

[21] Low-field magnetic susceptibility measurements were undertaken after each heating step to identify chemical alteration, but they failed to do so (Figure 7). Sample LV12E2 yielded an accurate paleointensity estimate (Table 2), and underwent little susceptibility variation during heating. Similarly, sample LV9A2 did not undergo much susceptibility change during heating; however, this sample overestimates the paleointensity by about 37%, and is excluded by the experimental alteration check, δ(CK). Sample MSH5B2 fails the δ(CK) criterion, but again had negligible susceptibility change during the experiment. This highlights the inadequacy of monitoring susceptibility changes during paleointensity experiments, but it also emphasizes the need to include pTRM checks, which are lacking in some approaches [e.g., *Dekkers and Böhnel*, 2006; *Biggin et al.*, 2007b].

[22] A further alteration check was made by considering sample lithology. All but one pumice sample failed at Láscar. Because of their friable nature and the ease with which pumices alter during heating, this is not surprising. Clast LV6G (sample LV6G1, Figure 1b) is an andesitic pumice, which had evidence of alteration (reddening at the edges) in the field, so it is plausible that alteration of pumiceous samples began from the onset of the paleointensity experiments. Of the accepted rock types, there is no lithological bias and each group of samples gives accurate paleointensity estimates. This provides confidence that the results are not biased by alteration in any particular lithology. Intensity values for each lithology are summarized in Table 4.

[23] *Draeger et al.* [2006] suggested that caution must be exercised when investigating paleointensities from materials that may have experienced late mineral crystallization through reheating, such as baked contacts and pyroclastic lithic clasts. This is because a chemical remanent magnetization (CRM) can produce linear trends on Arai plots [*Kono*, 1987; *Draeger et al.*, 2006]. A CRM intensity is typically lower than a TRM intensity [*McClelland*, 1996; *Draeger et al.*, 2006], and would therefore, produce an underestimate of the paleointensity during a Thellier-type experiment. Given the high quality and accuracy of the Láscar results, it is unlikely that these samples were affected by a CRM. However, the data from Mt. St. Helens and Vesuvius underestimate the paleointensity. Considering the poor quality of the line fits on the Arai plots for the Mt. St. Helens data (e.g.,

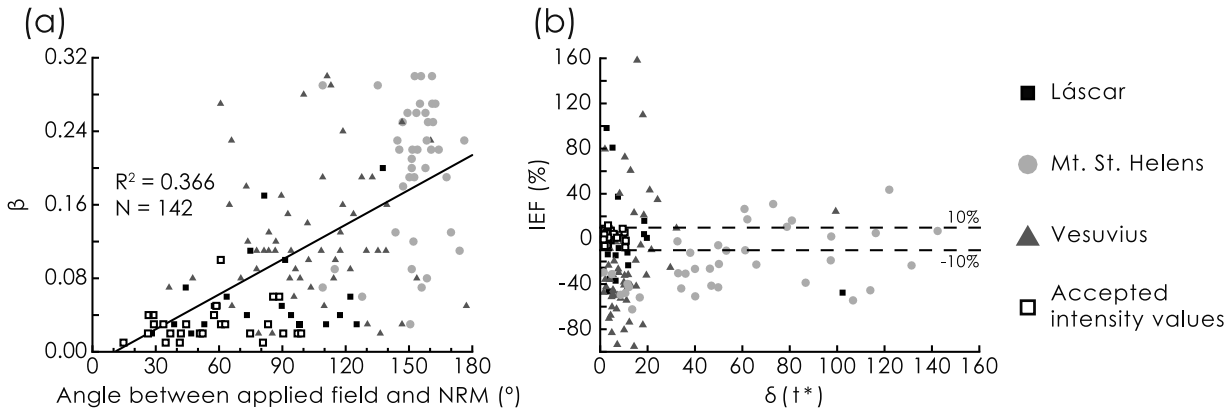

Figure 6. (a) Correlation of the angle between the applied laboratory field and the NRM direction and the scatter on an Arai plot (β). Although weak, the correlation is significant at the 0.01 significance level. This indicates that the scatter on the Arai plots is partially due to MD effects. (b) The $\delta(t^*)$ selection criterion for all samples. Few samples with $\delta(t^*) \geq 20$ have |IEF| $\leq$ 10%. Sample MSH4G5 (IEF(%) = −38.7, $\delta(t^*)$ = 338.4) is omitted for clarity.

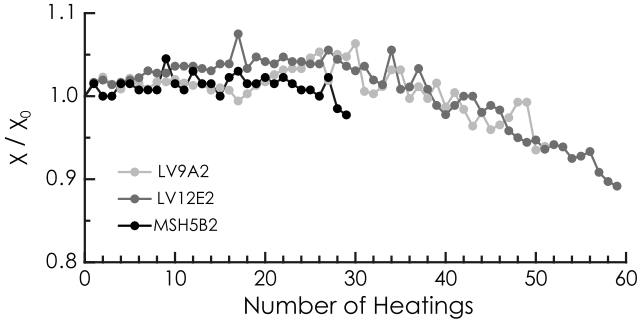

Figure 7. Low-field magnetic susceptibility measurements performed after each heating step during the paleointensity experiments. These measurements are not always diagnostic of chemical alteration during the paleointensity experiment. Sample LV9A2 was heated to a peak temperature of 580°C, sample LV12E2 was heated to 620°C, and sample MSH5B2 was heated to 390°C.

Figures 1e and 1f), little can be reliably inferred from this underestimate. At Vesuvius, the underestimation is greater and thermomagnetic evidence suggests a CRM in some clasts (e.g., Figure 2h). From FORC diagrams, we can identify MD grains and the presence of magnetic interactions (see section 7.2). Along with alteration during heating, these rock magnetic factors are equally plausible reasons for failure of the paleointensity determinations. Uncertainty associated with the expected paleointensity obtained from the CALS7K.2 model may account for the apparent paleointensity underestimate, and cannot be excluded.

[24] Paleointensity estimates for two Vesuvius samples that were suspected of having a CRM (samples CP4Q3B and CP6P3) both failed to meet selection criteria (Figure 8). Clast CP4Q has a Curie temperature that coincides with the emplacement temperature, which might suggest that the low temperature component is a CRM; the thermomagnetic curve for clast CP6P indicated the inversion of maghemite (Figure 2h). The Arai plot for sample CP4Q3B has a straight line segment that extends over the temperature range of the low temperature component, which yields an underestimate of the paleofield intensity and which agrees with the suggestion of *Draeger et al.* [2006]. The Arai plot for sample CP6P3 does not have a good linear segment, with pTRM checks failing at all temperatures. This indicates that alteration occurred throughout the paleointensity experiment, which suggests that the remanence carrier is chemically unstable, unlike the CRM behavior seen by *Draeger et al.* [2006]. These two cases highlight the extremes of CRM behavior, and the difficulty in conclusively identifying CRMs on the basis of paleointensity data.

7. Rock Magnetic Results

[25] Numerous authors have investigated the use of rock magnetic parameters as preselection tools for paleointensity analysis [e.g., *Cui et al.*, 1997; *Perrin*, 1998; *Carvallo et al.*, 2006]. Our large data set (142 samples) of paleointensity estimates from historic times provide an ideal opportunity to test suggested preselection approaches. Knowledge of the geomagnetic field strength allows these approaches to be assessed by directly comparing rock magnetic parameters with IEF(%), and enables comparison with respect to samples that pass the experimental selection criteria.

7.1. Hysteresis Analysis

[26] Hysteresis and back-field demagnetization measurements are among the most rapid rock magnetic measurements that can be made, which is appealing. Hysteresis parameters from all samples are plotted in Figures 9a–9d. Accepted paleointensity results and samples with low IEF(%) cover a wide range of hysteresis values. No correlation is observed between good paleointensity data and the rock magnetic parameters. Samples with low squareness (M_{rs}/M_s), high B_{cr}/B_c ratios, and low coercivities pass the experimental selection criteria and give accurate paleointensity estimates. These properties, however, would be expected to indicate poor paleomagnetic recording. *Michalk et al.* [2008] noted a weak correlation ($R^2 = 0.30$) between IEF(%) and squareness for historic volcanic samples from Mexico and Iceland. This correlation was observed only in paleointensity data from the multispecimen approach of *Dekkers and Böhnel* [2006] and not in data from IZZI experiments. They could not, however, exclude that this

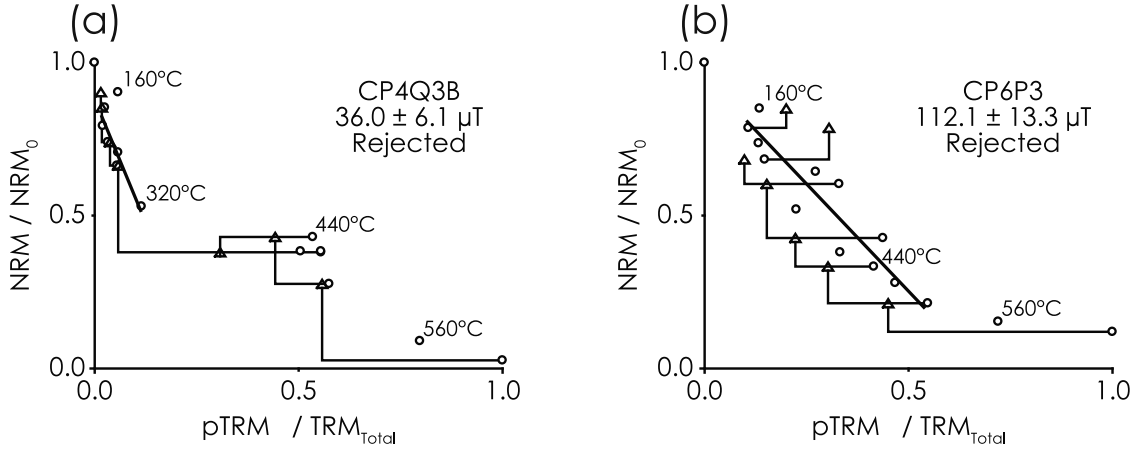

Figure 8. Arai plots for samples (a) CP4Q3B and (b) CP6P3 from Vesuvius. Both of these samples are likely to have a CRM. Symbols are the same as in Figure 1.

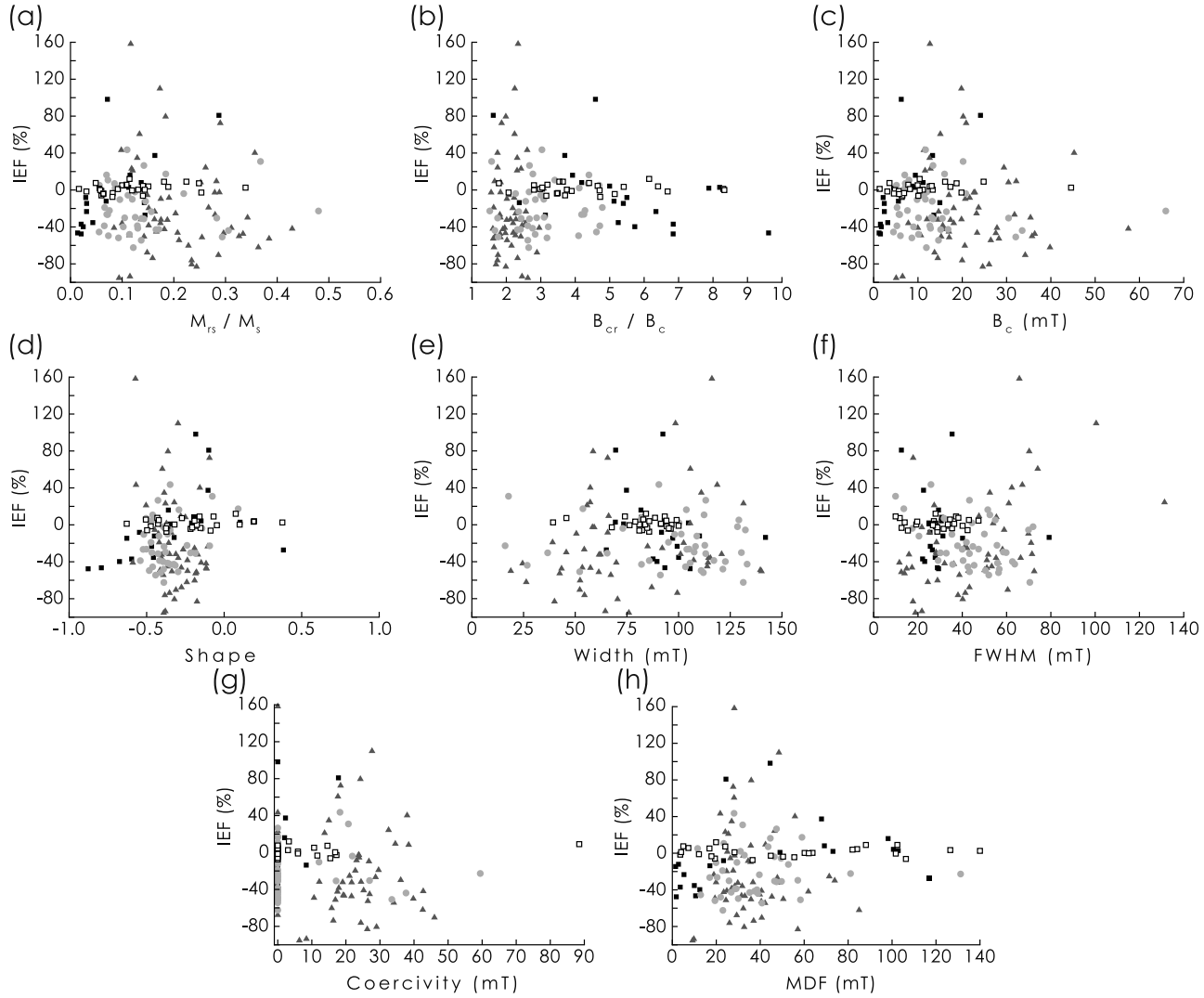

Figure 9. Rock magnetic selection criteria for paleointensity determinations, as investigated in this study for all samples. (a–d) Hysteresis parameters, (e–g) FORC parameters, and (h) median destructive field (MDF). See text for definitions of the FORC parameters. No significant correlation is evident between any magnetic parameter and IEF(%), or between any magnetic parameter and samples that pass the experimental paleointensity selection criteria. Symbols are the same as in Figure 6.

correlation is related to uncertainties in the expected field strength and not to MD effects. A similar correlation is observed in data reported by *Calvo et al.* [2002] and *Biggin and Thomas* [2003]; *Biggin and Thomas* [2003] attribute these correlations to the effects of pseudosingle domain (PSD)/MD grains. In particular, we observe no relation between IEF(%) and M_{rs}/M_s (Figure 9a).

[27] Data for some accepted samples appear toward the upper right-hand side of the Day plot [*Day et al.*, 1977] (Figure 10a), and may indicate a significant proportion of superparamagnetic (SP) grains. Overall, however, it is not possible to use a Day plot to discriminate between accepted and failed paleointensity results. A squareness-coercivity plot (Figure 10b) also fails to segregate results. *Fabian* [2003] suggested a plot of the shape parameter for hysteresis loops (which is sensitive to SP contributions) against B_{rh}/B_{cr} (which is sensitive to domain state; B_{rh} is the coercivity of remanent hysteretic magnetization [*Fabian and von Dobeneck*, 1997]), as shown in Figure 10c. Most of the studied samples have shape <0, which indicates that the hysteresis loops are largely pot-bellied [*Tauxe et al.*, 1996]. B_{rh}/B_{cr} has a narrow range of values and no distinction can be made to enable preselection of successful paleointensity samples.

[28] It has been noted by many authors [e.g., *Roberts et al.*, 1995, 2000; *Tauxe et al.*, 1996, 2002; *Muxworthy et al.*, 2003; *Williams et al.*, 2006] that various factors (e.g., grain-size distributions, magnetostatic interactions, mineralogy, grain shape, degree of grain stress, oxidation state) can influence hysteresis properties. These complicating factors prevent hysteresis data and related parameters from providing sufficiently unambiguous discrimination to provide a useful paleointensity preselection tool.

7.2. FORC Analysis

[29] It has been suggested that FORC diagrams [*Pike et al.*, 1999] could provide a more suitable screening technique for paleointensity experiments [*Roberts et al.*, 2000;

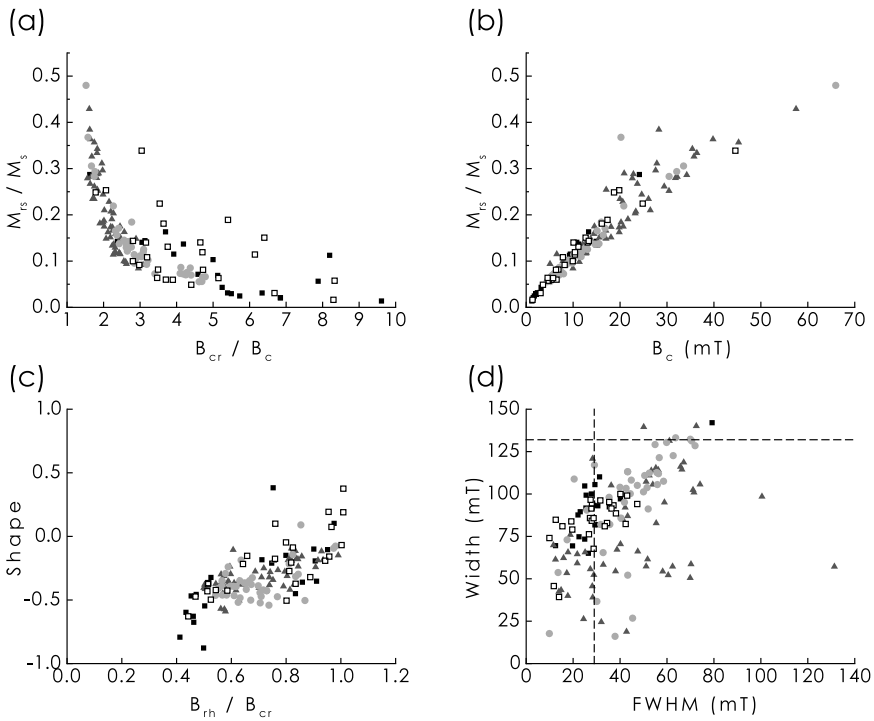

Figure 10. Typical rock magnetic biplots for data from the studied pyroclastic samples. Samples that pass the experimental selection criteria have no bias toward any diagnostic regions on any of the plots. The thresholds indicated by dashed lines in Figure 10d are from *Carvallo et al.* [2006]. Symbols are the same as in Figure 6.

Muxworthy et al., 2004]. *Carvallo et al.* [2006], on the basis of the analysis of about 200 mainly basaltic samples that had been subjected to paleointensity analysis, proposed selection criteria on the basis of FORC diagrams. They quantified FORC parameters to reject/accept samples for paleointensity experiments on the basis of the presence of interactions and/or a significant MD component. Use of three parameters enabled rejection of 32% of unsuccessful samples, with the remaining failures being attributed to thermal alteration (propensity to alteration is not related to rock magnetism). The PICRIT selection criteria of *Kissel and Laj* [2004] were used by *Carvallo et al.* [2006] to identify successful paleointensity determinations.

[30] The three parameters used by *Carvallo et al.* [2006] are the full-width at half maximum (FWHM) of the interaction field distribution at the peak of the FORC distribution; the spread of the FORC distribution along the $B_c = 0$ axis at 10% of the peak of the FORC distribution (called the width); and the bulk coercivity (B_c). The FWHM is an empirical parameter that quantifies the interaction field strength [*Muxworthy and Dunlop*, 2002]. Both the width and bulk coercivity are sensitive to magnetic domain state. Threshold acceptance values of FWHM $\leq$ 29 mT, width $\leq$ 132 mT, and $B_c \geq$ 5.4 mT exclude around one-third of unsuccessful samples, but also exclude about 8% of "successful" samples. *Carvallo et al.* [2006] noted that these excluded "successful" samples did not represent ideal paleointensity determinations.

[31] We encountered two difficulties when quantifying FORC diagrams with these parameters. First, many FORC diagrams have distribution peaks that are centered on the origin of the FORC diagram (e.g., Figures 11a and 11h), which results in $B_c = 0$, and makes this parameter difficult to use (Figure 9g). Second, the width parameter is difficult to measure because many samples have a contribution to the FORC distribution along the negative B_u axis at low coercivities, with the most extreme cases having near-vertical contours (Figure 11). This is a manifestation of single-domain (SD)/SP particles, as well as of domain walls with relaxation times close to the averaging time of the FORC measurement [*Pike et al.*, 2001]. This gives the width parameter an infinite value. To solve this problem, we assume a symmetrical FORC distribution and fold the width in the positive B_u direction to provide a width estimate that is similar to that used by *Carvallo et al.* [2006]. Where FORC distributions have peaks at the origin of the FORC diagram, the FWHM was folded in the same way. Samples without such distributions were used to check the validity of the folding process for the FWHM; the difference between the two approaches was minimal. No such check could be made for the width.

[32] Plots of the three FORC parameters and IEF(%) are shown in Figures 9e–9g. Coercivity provides no discrimination between good and bad paleointensity results. Width and FWHM do not correlate with IEF(%) or with successful results. When width is plotted against FWHM (Figure 10d), along with the cutoff values suggested by *Carvallo et al.* [2006], about 50% of the samples that pass the experimental criteria for acceptance of paleointensity data are excluded. A higher cutoff value of FWHM, i.e., about 50 mT includes all accepted results. *Wehland et al.* [2005] noted that some samples with successful paleointensity results have high

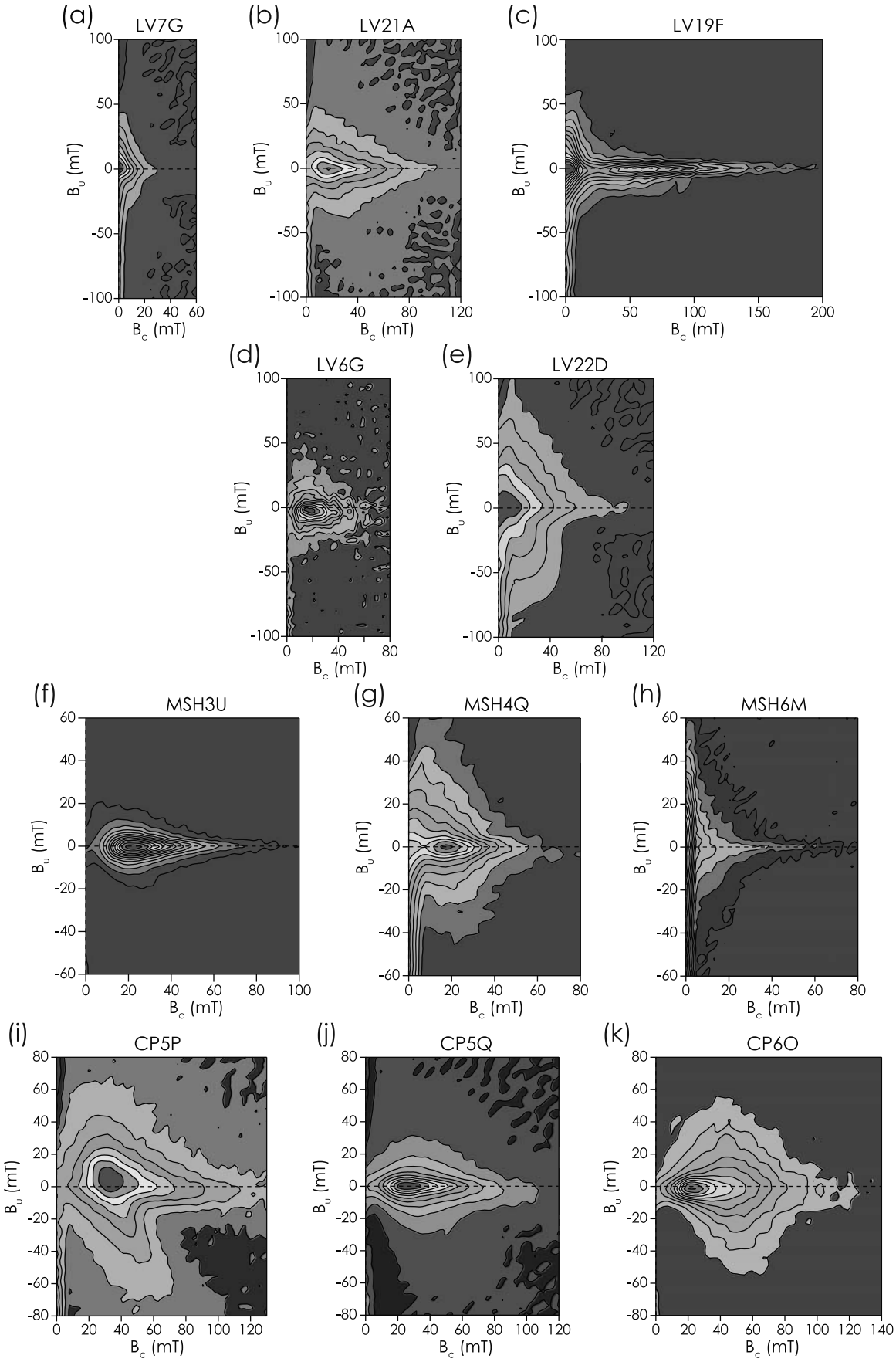
(a)
LV7G
(b)
LV21A
(c)
LV19F
(d)
LV6G
(e)
LV22D
(f)
MSH3U
(g)
MSH4Q
(h)
MSH6M
(i)
CP5P
(j)
CP5Q
(k)
CP6O
B_U (mT)
B_C (mT)

Figure 11

mean interaction fields. They suggested that the interplay of the interaction field and mean coercivity controls the influence of magnetic interactions on a paleointensity experiment. For our samples, no significant correlation could be identified between any coercivity parameter, FWHM and IEF(%). As is the case for hysteresis data, FORC data are inadequate for preselection for the studied samples. Reducing a FORC diagram to a few parameters loses a large amount of information. For example, in some cases, FWHM fails to quantify the true extent of magnetic interactions (e.g., Figure 11k). FWHM is a measure of the interaction field at the peak of the FORC distribution, in this case at $B_c \approx 20$ mT. However, the interaction field is much larger at higher coercivities.

[33] Despite the inability of FORC diagrams to enable preselection of samples that are suitable for paleointensity experiments in this study, they provide additional information to explain the possible causes of failure of paleointensity experiments. Narrow FORC distributions with peaks at B_c values of 20–30 mT are evident in Figures 11d, 11f, and 11j, which suggests the dominance of magnetically noninteracting SD magnetite. These samples should be ideal paleomagnetic recorders, so failure of paleointensity experiments is more likely to result from chemical alteration during the experiment; these three samples fail the δ(CK) criterion. Samples with MD- and PSD-like FORC diagrams (Figures 11e, 11i), respectively, both fail the δ(TR) pTRM tail check. Both, however, also fail the alteration check, which suggests that either: (1) both MD grains and alteration affected the paleointensity experiment; or (2) MD effects are not solely manifested as pTRM tails and can influence pTRM checks. Case 1 is the simplest explanation. Case 2 has been empirically demonstrated [*Biggin and Thomas*, 2003] and predicted theoretically [*Leonhardt et al.*, 2004b; *Biggin*, 2006; *Yu and Tauxe*, 2006]. *Yu and Tauxe* [2006] showed that MD remanence depends on the thermal prehistory of the sample, with pTRM intensity progressively increasing during multicycle heatings. This can affect pTRM checks and could produce a similar effect to alteration during a paleointensity experiment. These two scenarios are impossible to discriminate between with the data available. Samples from Láscar with MD-like FORC diagrams (e.g., Figure 11e), pass all of the experimental paleointensity selection criteria and yield accurate intensity estimates (e.g., sample LV19G; Table 2). This suggests a third possible explanation, in which there is a mixture of contrasting domain states where high field measurements such as FORCs indicate MD grains, whereas remanence measurements are dominated by SD grains, as suggested by *Carvallo et al.* [2006]. This could explain the lack of usefulness of FORC data for paleointensity preselection in this study.

7.3. AF Demagnetization

[34] AF demagnetization spectra can give an indication of the domain state and mineralogy of remanence carriers in paleomagnetic samples [*Dunlop and Özdemir*, 1997]. The median destructive field (MDF) is frequently cited as a measure of the hardness of remanence in paleomagnetic studies [e.g., *Dunlop and Özdemir*, 1997; *Carvallo et al.*, 2006]. IEF(%) versus MDF is plotted for all samples in Figure 9h. MDF ranges from 1.5 to >140 mT. A number of samples have MDF >100 mT, which indicates that significant (titano-) hematite is present in these samples. Samples that pass the experimental paleointensity selection criteria and those with low IEF(%) have MDFs that span the entire range of measured values. Samples with the most deviant IEF(%) values have MDFs of about 20–60 mT. *Carvallo et al.* [2006] measured the MDF of about 85% of their samples, which have a narrower range of values that extend up to about 80 mT. They suggested a minimum cutoff value of MDF = 12.9 mT. While this threshold excludes a number of our samples with failed paleointensity determinations, it also excludes good data and fails to remove most of the data from inaccurate samples. No MDF threshold value from our data could be used to isolate accepted from failed paleointensity results. An MDF selection criterion, therefore, does not provide suitable screening for paleointensity preselection for our samples.

7.4. Thermomagnetic Behavior

[35] Curie temperatures were measured for all clasts [*Paterson et al.*, 2010]. For the Láscar samples, T_c ranges from 397°C to 641°C; at Mt. St. Helens it ranges from 447°C to 634°C, and at Vesuvius it ranges from 533°C to 649°C. These Curie temperatures suggest the presence of low-Ti titanomagnetite, magnetite, and hematite. Thermomagnetic behavior is widely used for paleointensity preselection [e.g., *Goguitchaichvili et al.*, 1999; *Zhu et al.*, 2001; *Shcherbakova et al.*, 2008], with irreversible heating and cooling curves indicating thermal alteration. Thermomagnetic data from Láscar have both reversible and irreversible behavior (Figure 2) and there is no correlation between reversibility of the curves and samples that give acceptable paleointensity results. Thermomagnetic curves from Mt. St. Helens and Vesuvius both have reversible and irreversible behavior (Figures 2d–2i), while none of the paleointensity analyses yielded acceptable data. Lack of correlation between reversibility of thermomagnetic curves and successful paleointensity experiments has been noted by other authors [e.g., *Coe*, 1967b; *Coe and Grommé*, 1973; *Perrin*, 1998]. This lack of correlation can be explained in three ways: (1) alteration that gave rise to irreversible thermomagnetic curves is in a magnetic phase that carries an insignificant amount of NRM, so that while the alteration affects M_s, it has little influence on the paleointensity result; (2) alteration during the thermomagnetic measurement occurred above the maximum temperature used for the paleointensity estimate; or (3) alteration that affects the paleointensity experiment only occurs after repeated thermal cycling. The maximum heating step used in the paleointensity experiments was about 600°C, and thermomagnetic curves extend to at least 650°C with only one heating/cooling cycle, which makes it difficult to distin-

Figure 11. Example FORC diagrams from (a–e) Láscar, (f–h) Mt. St. Helens, and (i–k) Vesuvius. Samples LV7G, LV21A, and LV19F pass the experimental paleointensity selection criteria; samples LV6G and LV22D both fail. All samples from the latter two volcanoes fail to pass the experimental selection criteria. The measurement time for all experiments was 200 ms. The smoothing factor [cf., *Roberts et al.*, 2000] for each FORC diagram is 3.

guish between these possibilities. These factors make alteration during paleointensity experiments difficult to predict.

8. Discussion: Rock Magnetic Results

[36] The measured rock magnetic parameters in this study do not enable discrimination between samples that failed or that provided high quality paleointensity data. Previous attempts to use rock magnetism to preselect samples for paleointensity experiments have been assessed. The FORC parameter thresholds used by *Carvallo et al.* [2006] fail to isolate samples that yield accurate paleointensity values for the pyroclastic lithics studied here. It is possible, given that the Mt. St. Helens samples failed mainly due to chemical alteration, that our rock magnetic analysis might be biased by one data set. If we separately analyze data from the three different volcanoes, no correlation becomes evident. Lack of correlation between intensity results and rock magnetic data could also result from large lithological variations. Adequate preselection might, therefore, be achieved if only one rock type is considered. Andesite samples constitute the largest group in this study (48 samples; 23 from Láscar, 16 from Mt. St. Helens, and nine from Vesuvius), with 13 accepted paleointensity values. Isolating these samples and investigating the magnetic properties (for comparison, see Figures 9 and 10) yields no obvious correlation between magnetic properties and acceptable paleointensity data. The rock magnetic parameters for the andesites cover at least half the range of values for the entire sample set, and they often span the full range of values. This confirms that rock magnetic properties can vary widely within a lithology [e.g., *Chauvin et al.*, 2005; *Biggin et al.*, 2007a; *Michalk et al.*, 2008]. Questions may also be raised about the representativeness of the rock chips used to measure rock magnetic parameters compared to the larger samples used for paleointensity experiments. This can only be fully resolved by measuring several chips per clast, which negates any time advantage of preselection measurements.

[37] It appears that there is generally no correlation between high-field magnetic properties and low-field remanence behavior. For FORC and hysteresis measurements, this lack of correlation may be attributed to differences between high-field and remanence properties. However, remanence properties such as MDF are most likely dominated by mineralogical variations and not by magnetic domain state, which means that these parameters provide little useful information for paleointensity studies, especially in samples sets like the present one where the wide range of T_c values indicates considerable variation in magnetic mineralogy. Lack of correlation between the rock magnetic criteria and paleointensity results may be partially due to thermal alteration during the paleointensity experiments, or to the inequivalence of rock magnetic and paleointensity data for the variable studied lithologies in which variation in magnetic mineralogy might mask any relationship between domain state and paleointensity data.

9. Conclusions

[38] Using new experimental paleointensity selection criteria derived here (Table 3), we have accurately estimated the geomagnetic field intensity from pyroclastic lithic clasts from Volcán Láscar, Chile (24.3 ± 1.3 μT). When these criteria are applied to clasts from pyroclastic deposits at Mt. St. Helens and Vesuvius, all samples are rejected. Paleointensity experiments failed because of chemical alteration in nature and in the laboratory, MD effects, and potentially the effects of magnetic interactions. Threshold values of selection criteria were arbitrarily chosen on the basis of the available data. These new criteria, like previously published criteria, may not be universally applicable, but may serve as the basis for paleointensity studies using lithic clasts from pyroclastic deposits. Paleointensity criteria in this study are related to accuracy of the paleointensity estimate in a nondeterministic fashion. Further work is needed to refine paleointensity selection criteria; basing these criteria on paleointensity data from historic eruptions provides a useful measure of the accuracy of determinations, therefore, allowing development of optimal criteria.

[39] Rock magnetic measurements can help to constrain the cause(s) of failure of paleointensity experiments. However, numerical thresholds for key parameters fail to provide adequate preselection criteria for paleointensity experiments of the studied pyroclastic samples. This might be because the rock magnetic and paleointensity data involve high-field magnetic behavior and low-field remanence characteristics, which are often not equivalent, or because magnetic mineralogy is so variable that magnetic property variations due to mineralogy overwhelms those due to domain state.

[40] **Acknowledgments.** This study was funded by NERC grant NER/S/A/2005/13478 and by a Royal Society grant to A.R.M. We thank José Viramonte and Karen Paola Guzmán Montenegro for assistance with collecting samples from Láscar, and Lucia Gurioli and Francesca Lawley for assistance at Vesuvius. We also thank Roman Leonhardt and Andrew Biggin for constructive reviews that improved the paper.

References

Bardot, L., and E. McClelland (2000), The reliability of emplacement temperature estimates using palaeomagnetic methods: A case study from Santorini Greece, *Geophys. J. Int.*, *143*(1), 39–51, doi:10.1046/j.1365-246x.2000.00186.x.

Ben-Yosef, E., H. Ron, L. Tauxe, A. Agnon, A. Genevey, T. E. Levy, U. Avner, and M. Najjar (2008), Application of copper slag in geomagnetic archaeointensity research, *J. Geophys. Res.*, *113*, B08101, doi:10.1029/2007JB005235.

Biggin, A. J. (2006), First-order symmetry of weak-field partial thermoremanence in multidomain (MD) ferromagnetic grains: 2. Implications for Thellier-type palaeointensity determination, *Earth Planet. Sci. Lett.*, *245*, 454–470, doi:10.1016/j.epsl.2006.02.034.

Biggin, A. J., and D. N. Thomas (2003), The application of acceptance criteria to results of Thellier palaeointensity experiments performed on samples with pseudo-single-domain-like characteristics, *Phys. Earth Planet. Inter.*, *138*, 279–287, doi:10.1016/S0031-9201(03)00127-4.

Biggin, A. J., M. Perrin, and M. J. Dekkers (2007a), A reliable absolute palaeointensity determination obtained from a non-ideal recorder, *Earth Planet. Sci. Lett.*, *257*, 545–563, doi:10.1016/j.epsl.2007.03.017.

Biggin, A. J., M. Perrin, and J. Shaw (2007b), A comparison of a quasi-perpendicular method of absolute palaeointensity determination with other thermal and microwave techniques, *Earth Planet. Sci. Lett.*, *257*, 564–581, doi:10.1016/j.epsl.2007.03.016.

Calvo, M., M. Prévot, M. Perrin, and J. Riisager (2002), Investigating the reasons for the failure of palaeointensity experiments: A study on historical lava flows from Mt. Etna (Italy), *Geophys. J. Int.*, *149*(1), 44–63, doi:10.1046/j.1365-246X.2002.01619.x.

Carvallo, C., A. P. Roberts, R. Leonhardt, C. Laj, C. Kissel, M. Perrin, and P. Camps (2006), Increasing the efficiency of paleointensity analyses by selection of samples using first-order reversal curve diagrams, *J. Geophys. Res.*, *111*, B12103, doi:10.1029/2005JB004126.

Chauvin, A., Y. Garcia, P. Lanos, and F. Laubenheimer (2000), Paleointensity of the geomagnetic field recovered on archaeomagnetic sites from France, *Phys. Earth Planet. Inter.*, *120*, 111–136, doi:10.1016/S0031-9201(00)00148-5.

Chauvin, A., P. Roperch, and S. Levi (2005), Reliability of geomagnetic paleointensity data: The effects of the NRM fraction and concave-up behavior on paleointensity determinations by the Thellier method, *Phys. Earth Planet. Inter.*, *150*, 265–286, doi:10.1016/j.pepi.2004.11.008.

Coe, R. S. (1967a), Paleo-intensities of the Earth's magnetic field determined from Tertiary and Quaternary rocks, *J. Geophys. Res.*, *72*(12), 3247–3262, doi:10.1029/JZ072i012p03247.

Coe, R. S. (1967b), The determination of paleo-intensities of the Earth's magnetic field with emphasis on mechanisms which could cause non-ideal behavior in Thellier's method, *J. Geomagn. Geoelectr.*, *19*, 157–179.

Coe, R. S., and C. S. Grommé (1973), Comparison of three methods of determining geomagnetic paleointensities, *J. Geomagn. Geoelectr.*, *25*, 415–435.

Coe, R. S., S. Grommé, and E. A. Mankinen (1978), Geomagnetic paleointensities from radiocarbon-dated lava flows on Hawaii and the question of the Pacific nondipole low, *J. Geophys. Res.*, *83*(B4), 1740–1756, doi:10.1029/JB083iB04p01740.

Cottrell, R. D., and J. A. Tarduno (1999), Geomagnetic paleointensity derived from single plagioclase crystals, *Earth Planet. Sci. Lett.*, *169*, 1–5, doi:10.1016/S0012-821X(99)00068-0.

Cui, Y., K. L. Verosub, A. P. Roberts, and M. Kovacheva (1997), Mineral magnetic studies of archaeological samples: Implications for sample selection for paleointensity determinations, *J. Geomagn. Geoelectr.*, *49*, 567–585.

Day, R., M. Fuller, and V. A. Schmidt (1977), Hysteresis properties of titanomagnetites: Grain-size and compositional dependence, *Phys. Earth Planet. Inter.*, *13*, 260–267, doi:10.1016/0031-9201(77)90108-X.

Dekkers, M. J., and H. N. Böhnel (2006), Reliable absolute palaeointensities independent of magnetic domain state, *Earth Planet. Sci. Lett.*, *248*, 508–517, doi:10.1016/j.epsl.2006.05.040.

Draeger, U., M. Prévot, T. Poidras, and J. Riisager (2006), Single-domain chemical, thermochemical and thermal remanences in a basaltic rock, *Geophys. J. Int.*, *166*, 12–32, doi:10.1111/j.1365-246X.2006.02862.x.

Dunlop, D. J., and O. Özdemir (1997), *Rock Magnetism: Fundamentals and Frontiers, Cambridge Stud. Magn.*, vol. 3, Cambridge Univ. Press, New York.

Fabian, K. (2003), Some additional parameters to estimate domain state from isothermal magnetization measurements, *Earth Planet. Sci. Lett.*, *213*, 337–345, doi:10.1016/S0012-821X(03)00329-7.

Fabian, K., and T. von Dobeneck (1997), Isothermal magnetization of samples with stable Preisach function: A survey of hysteresis, remanence, and rock magnetic parameters, *J. Geophys. Res.*, *102*(B8), 17,659–17,677, doi:10.1029/97JB01051.

Fisher, R. V., and H. U. Schmincke (1984), *Pyroclastic Rocks*, 472 pp., Springer, Berlin.

Genevey, A., and Y. Gallet (2002), Intensity of the geomagnetic field in western Europe over the past 2000 years: New data from ancient French pottery, *J. Geophys. Res.*, *107*(B11), 2285, doi:10.1029/2001JB000701.

Genevey, A., Y. Gallet, and J.-C. Margueron (2003), Eight thousand years of geomagnetic field intensity variations in the eastern Mediterranean, *J. Geophys. Res.*, *108*(B5), 2228, doi:10.1029/2001JB001612.

Goguitchaichvili, A., N. Roberts, M. Prévot, and J. Thompson (1999), An attempt to determine the absolute geomagnetic field intensity in Southwestern Iceland during the Gauss-Matuyama reversal, *Phys. Earth Planet. Inter.*, *115*, 53–66, doi:10.1016/S0031-9201(99)00064-3.

Guyodo, Y., and J.-P. Valet (1996), Relative variations in geomagnetic intensity from sedimentary records: The past 200000 years, *Earth Planet. Sci. Lett.*, *143*, 23–36, doi:10.1016/0012-821X(96)00121-5.

Harrison, R. J., and J. M. Feinberg (2008), FORCinel: An improved algorithm for calculating first-order reversal curve distributions using locally weighted regression smoothing, *Geochem. Geophys. Geosyst.*, *9*, Q05016, doi:10.1029/2008GC001987.

Hill, M. J., and J. Shaw (2000), Magnetic field intensity study of the 1960 Kilauea lava flow, Hawaii, using the microwave palaeointensity technique, *Geophys. J. Int.*, *142*(2), 487–504, doi:10.1046/j.1365-246x.2000.00164.x.

International Association of Geomagnetism (2005), Aeronomy, 2005. The 10th generation international geomagnetic reference field, *Geophys. J. Int.*, *161*, 561–565, doi:10.1111/j.1365-246X.2005.02641.x.

Kent, D. V., D. Ninkovitch, T. Pescatore, and R. S. J. Sparks (1981), Palaeomagnetic determination of emplacement temperature of the Vesuvius AD 79 pyroclastic deposits, *Nature*, *290*, 393–396, doi:10.1038/290393a0.

Kissel, C., and C. Laj (2004), Improvements in procedure and paleointensity selection criteria (PICRIT-03) for Thellier and Thellier determinations: Application to Hawaiian basaltic long cores, *Phys. Earth Planet. Inter.*, *147*, 155–169, doi:10.1016/j.pepi.2004.06.010.

Knudsen, M. F., P. Riisager, F. Donadini, I. Snowball, R. Muscheler, K. Korhonen, and L. J. Pesonen (2008), Variations in the geomagnetic dipole moment during the Holocene and the past 50 kyr, *Earth Planet. Sci. Lett.*, *272*, 319–329, doi:10.1016/j.epsl.2008.04.048.

Kono, M. (1987), Changes in TRM and ARM in a basalt due to laboratory heating, *Phys. Earth Planet. Inter.*, *46*, 1–8, doi:10.1016/0031-9201(87)90167-1.

Korhonen, K., F. Donadini, P. Riisager, and L. J. Pesonen (2008), GEOMAGIA50: An archeointensity database with PHP and MySQL, *Geochem. Geophys. Geosyst.*, *9*, Q04029, doi:10.1029/2007GC001893.

Korte, M., and C. G. Constable (2005), Continuous geomagnetic field models for the past 7 millennia: 2. CALS7K, *Geochem. Geophys. Geosyst.*, *6*, Q02H16, doi:10.1029/2004GC000801.

Kovacheva, M., and A. Toshkov (1994), Geomagnetic field variations as determined from Bulgarian archaeomagnetic data, *Surv. Geophys.*, *15*, 673–701, doi:10.1007/BF00666090.

Lanza, R., and E. Zanella (2003), Paleomagnetic secular variation at Vulcano (Aeolian Islands) during the last 135 kyr, *Earth Planet. Sci. Lett.*, *213*, 321–336, doi:10.1016/S0012-821X(03)00326-1.

Leonhardt, R. (2006), Analyzing rock magnetic measurements: The RockMagAnalyzer 1.0 software, *Comput. Geosci.*, *32*, 1420–1431, doi:10.1016/j.cageo.2006.01.006.

Leonhardt, R., C. Heunemann, and D. Krása (2004a), Analyzing absolute paleointensity determinations: Acceptance criteria and the software ThellierTool4.0, *Geochem. Geophys. Geosyst.*, *5*, Q12016, doi:10.1029/2004GC000807.

Leonhardt, R., D. Krása, and R. S. Coe (2004b), Multidomain behavior during Thellier paleointensity experiments: A phenomenological model, *Phys. Earth Planet. Inter.*, *147*, 127–140, doi:10.1016/j.pepi.2004.01.009.

Leonhardt, R., D. B. Dingwell, J. Matzka, and A. R. L. Nichols (2006), Cooling rate correction of paleointensity determination for volcanic glasses by relaxation geospeedometry, *Earth Planet. Sci. Lett.*, *243*, 282–292, doi:10.1016/j.epsl.2005.12.038.

Levi, S. (1977), Effect of magnetite particle-size on paleointensity determinations of geomagnetic field, *Phys. Earth Planet. Inter.*, *13*, 245–259, doi:10.1016/0031-9201(77)90107-8.

McClelland, E. (1996), Theory of CRM acquired by grain growth, and its implications for TRM discrimination and palaeointensity determination in igneous rocks, *Geophys. J. Int.*, *126*, 271–280, doi:10.1111/j.1365-246X.1996.tb05285.x.

McClelland, E., and J. C. Briden (1996), An improved methodology for Thellier-type paleointensity determination in igneous rocks and its usefulness for verifying primary thermoremanence, *J. Geophys. Res.*, *101*(B10), 21,995–22,013, doi:10.1029/96jb02113.

Michalk, D. M., A. R. Muxworthy, H. N. Böhnel, J. Maclennan, and N. R. Nowaczyk (2008), Evaluation of the multispecimen parallel differential pTRM method: A test on historical lavas from Iceland and Mexico, *Geophys. J. Int.*, *173*, 409–420, doi:10.1111/j.1365-246X.2008.03740.x.

Muxworthy, A. R., and D. J. Dunlop (2002), First-order reversal curve (FORC) diagrams for pseudo-single-domain magnetites at high temperature, *Earth Planet. Sci. Lett.*, *203*, 369–382, doi:10.1016/S0012-821X(02)00880-4.

Muxworthy, A. R., W. Williams, and D. Virdee (2003), Effect of magnetostatic interactions on the hysteresis parameters of single-domain and pseudo-single-domain grains, *J. Geophys. Res.*, *108*(B11), 2517, doi:10.1029/2003JB002588.

Muxworthy, A. R., D. Heslop, and W. Williams (2004), Influence of magnetostatic interactions on first-order-reversal-curve (FORC) diagrams: A micromagnetic approach, *Geophys. J. Int.*, *158*, 888–897, doi:10.1111/j.1365-246X.2004.02358.x.

Paterson, G. A., A. P. Roberts, A. R. Muxworthy, C. Mac Niocaill, L. Gurioli, J. G. Viramonté, C. Navarro, and S. Weider (2010), Paleomagnetic determination of emplacement temperatures of pyroclastic deposits: An under-utilized tool, *Bull. Volcanol.*, doi:10.1007/s00445-009-0324-4, in press.

Perrin, M. (1998), Paleointensity determination, magnetic domain structure, and selection criteria, *J. Geophys. Res.*, *103*(B11), 30,591–30,600, doi:10.1029/98JB01466.

Perrin, M., and E. Schnepp (2004), IAGA paleointensity database: Distribution and quality of the data set, *Phys. Earth Planet. Inter.*, *147*, 255–267, doi:10.1016/j.pepi.2004.06.005.

Petrovský, E., and E. Kapička (2006), On determination of the Curie point from thermomagnetic curves, *J. Geophys. Res.*, *111*, B12S27, doi:10.1029/2006JB004507.

Pick, T., and L. Tauxe (1993), Geomagnetic palaeointensities during the Cretaceous normal superchron measured using submarine basaltic glass, *Nature*, *366*, 238–242, doi:10.1038/366238a0.

Pike, C. R., A. P. Roberts, and K. L. Verosub (1999), Characterizing interactions in fine magnetic particle systems using first order reversal curves, *J. Appl. Phys.*, *85*, 6660–6667, doi:10.1063/1.370176.

Pike, C. R., A. P. Roberts, and K. L. Verosub (2001), First-order reversal curve diagrams and thermal relaxation effects in magnetic particles,

Geophys. J. Int., *145*(3), 721–730, doi:10.1046/j.0956-540x.2001.01419.x.

Roberts, A. P., Y. L. Cui, and K. L. Verosub (1995), Wasp-waisted hysteresis loops: Mineral magnetic characteristics and discrimination of components in mixed magnetic systems, *J. Geophys. Res.*, *100*(B9), 17,909–17,924, doi:10.1029/95jb00672.

Roberts, A. P., C. R. Pike, and K. L. Verosub (2000), First-order reversal curve diagrams: A new tool for characterizing the magnetic properties of natural samples, *J. Geophys. Res.*, *105*(B12), 28,461–28,475, doi:10.1029/2000JB900326.

Selkin, P. A., and L. Tauxe (2000), Long-term variations in palaeointensity, *Philos. Trans. R. Soc. London*, *358*, 1065–1088, doi:10.1098/rsta.2000.0574.

Shaw, J. (1974), A new method of determining the magnitude of the palaeomagnetic field: Application to five historic lavas and five archaeological samples, *Geophys. J. R. Astron. Soc.*, *39*, 133–141, doi:10.1111/j.1365-246X.1974.tb05443.x.

Shcherbakova, V., N. V. Lubnina, V. P. Shcherbakov, S. Mertanen, G. V. Zhidkov, T. I. Vasilieva, and V. A. Tsel'movich (2008), Palaeointensity and palaeodirectional studies of early Riphaean dyke complexes in the Lake Ladoga region (Northwestern Russia), *Geophys. J. Int.*, *175*, 433–448, doi:10.1111/j.1365-246X.2008.03859.x.

Smithsonian Institution (1980), Mount St. Helens, *Sci. Event Alert Network (SEAN) Bull.*, *5*, Smithsonian Inst., Washington, D. C.

Smithsonian Institution (1993), Láscar, *Sci. Event Alert Network (SEAN) Bull.*, *18*, Smithsonian Inst., Washington, D. C.

Tarduno, J. A., R. D. Cottrell, and A. V. Smirnov (2006), The paleomagnetism of single silicate crystals: Recording geomagnetic field strength during mixed polarity intervals, superchrons, and inner core growth, *Rev. Geophys.*, *41*, RG1002, doi:10.1029/2005RG000189.

Tarling, D. H. (1983), *Palaeomagnetism: Principles and Applications in Geology, Geophysics and Archaeology*, 379 pp., Chapman and Hall, London.

Tauxe, L., T. A. T. Mullender, and T. Pick (1996), Potbellies, wasp-waists, and superparamagnetism in magnetic hysteresis, *J. Geophys. Res.*, *101*(B1), 571–583, doi:10.1029/95JB03041.

Tauxe, L., H. N. Bertram, and C. Seberino (2002), Physical interpretation of hysteresis loops: Micromagnetic modeling of fine particle magnetite, *Geochem. Geophys. Geosyst.*, *3*(10), 1055, doi:10.1029/2001GC000241.

Thellier, E., and O. Thellier (1959), Sur l'intensité du champ magnétique terrestre dans le passé historique et géologique, *Ann. Geophys.*, *15*, 285–376.

Walton, D., J. Shaw, J. Share, and J. Hakes (1992), Microwave demagnetization, *J. Appl. Phys.*, *71*, 1549–1551, doi:10.1063/1.351230.

Wehland, F., R. Leonhardt, F. Vadeboin, and E. Appel (2005), Magnetic interaction analysis of basaltic samples and pre-selection for absolute palaeointensity measurements, *Geophys. J. Int.*, *162*, 315–320, doi:10.1111/j.1365-246X.2005.02429.x.

Williams, W., A. R. Muxworthy, and G. A. Paterson (2006), Configurational anisotropy in single-domain and pseudosingle-domain grains of magnetite, *J. Geophys. Res.*, *111*, B12S13, doi:10.1029/2006JB004556.

Yu, Y. J., and L. Tauxe (2005), Testing the IZZI protocol of geomagnetic field intensity determination, *Geochem. Geophys. Geosyst.*, *6*, Q05H17, doi:10.1029/2004GC000840.

Yu, Y. J., and L. Tauxe (2006), Effect of multicycle heat treatment and prehistory dependence on partial thermoremanence (pTRM) and pTRM tails, *Phys. Earth Planet. Inter.*, *157*, 196–207, doi:10.1016/j.pepi.2006.04.006.

Yu, Y. J., L. Tauxe, and A. Genevey (2004), Toward an optimal geomagnetic field intensity determination technique, *Geochem. Geophys. Geosyst.*, *5*, Q02H07, doi:10.1029/2003GC000630.

Zhu, R., D. Li, Q. Li, Y. Pan, and J. Shaw (2001), Geomagnetic palaeointensity just prior to the Cretaceous normal superchron, *Phys. Earth Planet. Inter.*, *128*, 207–222, doi:10.1016/S0031-9201(01)00287-4.

C. Mac Niocaill, Department of Earth Sciences, University of Oxford, Parks Road, Oxford OX1 3PR, UK.

A. R. Muxworthy, Department of Earth Science and Engineering, Imperial College London, South Kensington Campus, London SW7 2AZ, UK.

G. A. Paterson and A. P. Roberts, National Oceanography Centre, University of Southampton, Southampton SO14 3ZH, UK. (gap1@noc.soton.ac.uk)